SPSD II

ANTHROPOGENIC AND BIOGENIC INFLUENCES ON THE OXIDATION CAPACITY OF THE ATMOSPHERE

J.-F. MULLER, C. VINCKIER, J. PEETERS, E. ARIJS

PART 2

GLOBAL CHANGE, ECOSYSTEMS AND BIODIVERSITY ⎯⎯⎯ **ATMOSPHERE AND CLIMATE**

MARINE ECOSYSTEMS AND BIODIVERSITY

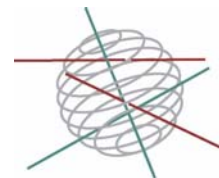TERRESTRIAL ECOSYSTEMS AND BIODIVERSITY

NORTH SEA

ANTARCTICA

BIODIVERSITY

.be

**SCIENTIFIC SUPPORT PLAN FOR A SUSTAINABLE DEVELOPMENT POLICY
(SPSD II)**

Part 2:
Global Change, Ecosystems and Biodiversity

FINAL REPORT

**ANTHROPOGENIC AND BIOGENIC INFLUENCES ON THE OXIDATION
CAPACITY OF THE ATMOSPHERE**

EV/06

Promoters
J.-F. Muller / IASB-BIRA
C. Vinckier / KULeuven-Laboratory for Physical and Analytical Chemistry
J. Peeters / KULeuven-Division of Quantum Chemistry and Physical Chemistry
E. Arijs / BIRA-IASB

Scientific collaborators
M. Capouet, S. Wallens, T. Stavrakou / IASB-BIRA
H. Vankerckhoven, V. Van Den Bergh, H. Coeckelberghs,
F. Compernolle / KULeuven-Laboratory for Physical and Analytical Chemistry
L. Vereecken, G. Fantechi, I. Hermans, C. Coeck, T.L. Nguyen, P.A. Jacobs / KULeuven-
Division of Quantum Chemistry and Physical Chemistry
C. Amelynck, N. Schoon / BIRA-IASB

August 2005

BELGIAN SCIENCE POLICY

TABLE OF CONTENTS

ABSTRACT

The composition of the troposphere is strongly affected by biogenic and anthropogenic emissions of chemical compounds, including hydrocarbons, carbon monoxide, and the nitrogen oxides. The emissions of non-methane hydrocarbons, in particular, have a large impact on the oxidizing capacity of the atmosphere (which determines the fate and lifetime of a large number of pollutants and greenhouse gases) and on the budget and distribution of tropospheric ozone and aerosols. These compounds are therefore key actors in both air quality and climate change issues. The terrestrial vegetation represents by far their largest source on the global scale. Foliar emissions include isoprene (C_5H_8), monoterpenes ($C_{10}H_{16}$) and other compounds.

Whereas the chemistry of isoprene is relatively well established and realistic mechanisms for its atmospheric oxidation are included in many chemistry-transport models, the degradation of monoterpenes remains speculative at this stage. Due to the low volatility of a number of their oxidation products, monoterpenes are considered as important precursors of organic aerosols in the atmosphere. In addition, acetone, a known oxidation product of several monoterpenes, is believed to be an important source of radicals in the region of the tropopause, and to influence the budget of ozone and hydroxy radicals. Due to the cold temperatures and low pressures prevailing in this region, however, the precise influence of acetone and other oxygenated organic compounds is uncertain, due to the possibility of unexpected behaviour of key reactions in the conditions typical of the tropopause.
In this project, the impact of monoterpenes and other key organic compounds on the formation of oxidants and aerosols has been investigated through a combination of laboratory, theoretical and modelling studies.

Experimental techniques developed in Leuven in a previous project (under the SPSD 1 programme) have been further elaborated in this project by both Katholieke Universiteit Leuven (team of Chris Vinckier, C.V.) and the Belgian Institute for Space Aeronomy (team of Etienne Arijs, E.A.) to study the reaction of important monoterpenes (α- and β-pinene, Δ^3-carene and limonene) with hydroxyl radicals (OH) in presence of oxygen (20%) and under reaction pressures of 50-200 Torr. These reactions have been studied in fast flow reactors equipped with a microwave discharge as clean OH radical source. In order to clarify the role of the terpene chemistry a major challenge is the identification and quantification of the semi-volatile compounds formed as oxidation products.

In the study conducted in Leuven (C.V.), these products are collected on a liquid nitrogen trap and 'derivatized' prior to analysis. Reaction products are identified and quantified using two complementary techniques, HPLC-MS and HPLC-DAD. New ionization techniques have been explored (for HPLC-MS), and appropriate analytical methods have been developed. The following products are found in the reaction of β-pinene with OH: formaldehyde, acetaldehyde, acetone, trans-3-hydroxynopinone, nopinone, perilla alcohol, perillaldehyde and myrtanal, with formaldehyde and nopinone the most important ones. Caronaldehyde is identified as the most important reaction product in the Δ^3-carene+OH reaction, together with formaldehyde and acetone. For limonene, endolim is identified as the dominant product together with 4-AMCH, formaldehyde and acetone. The relative yields have been determined under a variety of experimental conditions. The impact of variations in the reaction time, reaction pressure, nitric oxide concentration, initial hydrogen concentration and OH/terpene concentration ratio on the product yields has been investigated. Finally, a kinetic reaction study of the α-pinene+OH reaction has been carried out. It suggests that a large number of polyfunctional products (such as hydroxyperoxides) could not be detected, possibly representing as much as 50% of the total on a molar basis. This problem should be solved in future studies by using our newly developed HPLC-MS^n technique coupled with a suitable ionisation source (ESI or APCI).

In the study conducted in Brussels by the team of Etienne Arijs (E.A.), the organic reactant and its products are led into a chemical ionization mass spectrometer (CIMS) where they react with appropriate precursor ions (e.g. H_3O^+, NO^+, CH_3O^- or SF_6^-). The ion/molecule reactions result in specific product ions which are the 'fingerprints' of the molecules to be detected. A low pressure fast-flow reactor has been used in the first stage of the project. It has been replaced later on by a high pressure turbulent flow reactor, which combines the advantage of efficient mixing with the possibility to perform experiments at higher pressures (200 Torr). Since absolute and accurate CIMS-based quantification requires the knowledge of the rate constants and product ion distributions of the relevant ion/molecule reactions, these parameters have been measured in a selected ion flow tube instrument (SIFT), and confirmed by theoretical calculations in collaboration with the team of Jozef Peeters (J.P.) at the Katholieke Universiteit Leuven. The characterization of ion/molecule reactions for the monoterpenes, for their oxidation products and for a large number of other oxygenated organics constituted an important part of the work in this project. The absolute yields of the main oxidation products (acetone, formaldehyde, pinonaldehyde and nopinone) in the reactions of α-pinene (at 2 and 50 Torr) and β-pinene (at 200 Torr) with OH have been determined in varied conditions.

An extensive theoretical and mechanistic study of the OH-initiated oxidation of α-pinene, pinonaldehyde and β-pinene has been conducted in Leuven by the team of Jozef Peeters (J.P.). On objective theoretical grounds, the fate of the many oxy radicals involved in these mechanisms has been predicted. This work is based on objective chemical kinetics knowledge, or quantitative structure-activity relationships (SARs)—some of which were further developed in this project—and *ab initio* or density functional theory (DFT) barrier heights and rotation/vibration parameters, in combination with statistical rate theories. Based on these studies, we have developed detailed mechanisms for the OH-initiated oxidation of α-pinene, pinonaldehyde and β-pinene. Our mechanisms describe the chemistry of all existing OH addition and H abstraction pathways. This work led us to discover novel reaction pathways, which were entirely overlooked so far. These non-traditional 'ring closure' reactions of oxy and peroxy radicals were never reported in laboratory conditions, but are nonetheless important or even crucial in the oxidation of isoprene and many monoterpenes in the real atmosphere, due to the lower concentrations of radicals in the atmosphere compared to the laboratory. In typical experimental setups, the ring closure reactions are usually outrun by other reactions.

The total product yields (obtained by propagating the product fractions in each step of the mechanism) are in good general agreement with experimental values, with the exception of the formaldehyde yield in the oxidation of pinonaldehyde, which is about one order of magnitude lower than the only reported experimental result (very high value that remains unconfirmed). We have performed a critical evaluation of the few mechanisms available in the literature, especially concerning the steps leading to the main products. The same methods have been also applied, to a more limited extent, to the ozonolysis of α-pinene.

The α-pinene mechanism described above has been generalized and implemented in a chemical 'box' model by the team of J.-F. Müller (J-F.M.) at the Belgian Institute for Space Aeronomy and the team of J.P. in Leuven. We have estimated the rates of the photolysis processes and of the peroxy radical reactions involved in this mechanism on the basis of a detailed literature survey. The impact of the numerous permutation reactions of peroxy radicals is accounted for by including the reactions of each individual radical with pseudo-species representing radical classes. We have validated the mechanism and the model against the series of ~40 photooxidation experiments performed by Nozière *et al.* (1999). The model performs well for all species, except acetone in the absence of NO. This is a probable consequence of the non-explicit treatment of the chemistry following specific reactions in the mechanism (ring closure, oxidation of primary products). Based on the explicit

mechanism (2000 reactions), a reduced mechanism of only ~100 reactions has been designed, suitable for use in 3-dimensional models.

We have developed a model for calculating the partitioning between the gas and particulate phases of the monoterpene degradation products (J-F.M. team at Belgian Institute for Space Aeronomy). It relies on the estimation of the vapour pressures of organic compounds according to group contribution principles. The method has been adjusted by using a large set of vapour pressure measurements. It is found to be of comparable or better performance than a widely used prediction method, UNIFAC. Since pinic acid can be expected to be mostly present as dimer in laboratory conditions, we suggest that the partial vapour pressure of this dimer should be close to the experimental subcooled vapour pressure for pinic acid. Results from ozonolysis experiments have been used to test both the mechanism and the gas-particle partitioning model. The total aerosol concentration observed by one group is fairly well reproduced by the model, in contrast with the yields observed by another group at higher temperatures.

We have determined the product distribution of the controversial elementary reaction of acetone with OH radicals in flow reactors by molecular beam sampling mass spectrometry in KULeuven (J.P.) and by the CIMS technique in the Belgian Institute for Space Aeronomy (E.A.; see above). Recent reports had indicated that this reaction proceeds for ~50% by a mechanism leading to acetic acid, with potentially significant implications for the chemistry of the upper troposphere. However, our direct measurements of the acetic acid yield show unequivocally that this reaction path is minor (<5%) and that the H-abstraction path is the only route of importance. We have also performed theoretical calculations (J.P.) which confirm this result and explain the negative temperature dependence of the reaction rate at low temperatures.

Similarly, we have shown (J.P.) by direct measurements that the elementary reactions of OH with acetaldehyde and propionaldehyde proceed for >90% by H-abstraction and, again contrary to earlier reports, do not yield acids in any significant amount; this finding is of key importance for the budget of peroxyacylnitrates (PAN) in the atmosphere. The elementary reaction of OH with acetic acid was found to yield directly 65% CH_3 + CO_2, consistent with our theoretical predictions; in addition, we confirmed the strongly negative temperature dependence of the total rate coefficient, of importance for Upper Troposphere chemistry models.

Carbonyls are usually assumed to either photolyse or react with OH radicals in the atmosphere. In this project, we have shown by state-of-the-art theoretical calculations that their reactions with HO_2 radicals might play a significant role in the vicinity of the tropopause (teams of J.P. and J-F.M.). The peroxy radicals formed by these reactions can either decompose back to the original reactants or undergo other reactions leading for the largest part to the formation of carboxylic acids. The strong temperature dependence of the decomposition rates explains the negligible impact of the overall reaction sequence throughout most of the troposphere (at T>~220 K). We have assessed the potential significance of these reactions for formaldehyde and acetone by three-dimensional model calculations. Their contribution to the overall sink of these compounds is calculated to reach ~30% or more in the tropical tropopause region, with significant effects on the levels of OH and HO_2 radicals.

We have developed a detailed vegetation canopy model for estimating the temperature and radiative fluxes at the leaf level (J-F.M.). By this way, the widely used algorithms of Guenther *et al*. (1995) for the calculation of biogenic emissions could be evaluated against flux measurements from selected campaigns, and alternative algorithms have been tested. A good model performance is noted, except at an Amazonian site and at a mid-latitude site in spring and autumn, where the model largely overestimates the fluxes. Based on the canopy model and on available climatologies for meteorological and vegetation parameters, the global emissions of isoprene and monoterpenes have been estimated at a resolution of 0.5° in both latitude and longitude. The calculations show that the leaf/air temperature difference might enhance the emissions by 30% or more in subtropical areas during the dry season.

An alternative approach for estimating the emissions of reactive compounds has been developed, using a global chemistry-transport model (J-F.M.). The emissions in the model are optimized by minimizing the bias between the model predictions and a set of atmospheric observations. The innovative aspect of our study lies in the use of the adjoint model technique. This method has been successfully applied to the optimization of the carbon monoxide and nitrogen oxides emissions. The method is also appropriate for estimating the emissions of biogenic volatile organic compounds based on satellite observations of their oxidation by-products formaldehyde and carbon monoxide.

Finally, the global model IMAGES has been used (J-F.M.) to predict the composition of the troposphere for present-day as well as for future conditions, in the framework of model intercomparisons supervised by the Intergovernmental Panel on Climate Change (IPCC). These simulations are based on different anthropogenic emission scenarios. These scenarios reflect possible future population, economic and technological changes, including the effect of regulations aimed at mitigating the adverse effects of these emissions. The results of these studies are part of the latest IPCC Third Assessment Report - Climate Change 2001 (IPCC-TAR report).

Keywords: troposphere, ozone, secondary organic aerosols, biogenic emissions, volatile organic compounds, oxidation mechanisms, oxidizing capacity of the atmosphere

1. INTRODUCTION

The composition of the troposphere is strongly affected by biogenic and anthropogenic emissions of chemically reactive compounds, including hydrocarbons, carbon monoxide, and the nitrogen oxides. The anthropogenic emissions of these compounds – resulting from the burning of fossil fuels, industrial and agricultural activities, and vegetation fires – are known to deteriorate air quality, with important effects on human health and agricultural yields, and to enhance the build-up of greenhouse gases (e.g. ozone) and aerosols, with important effects on climate.

Three-dimensional chemistry/transport models (CTMs) are used to estimate the impact of human-induced emissions on the tropospheric composition. For this reason, they are considered essential to policy-makers in their efforts to design international conventions on air quality and climate change (like the Kyoto Protocol[1]) aiming at the mitigation of these effects. There are, however, large uncertainties in these calculations, and possibly important gaps in our representation of the processes involved.

The present project involves teams led by J.-F. Muller (Brussels), C. Vinckier (Leuven), J. Peeters (Leuven), and E. Arijs (Brussels). Its main objective is the reduction of uncertainties, in particular those associated with

1/ the emissions of ozone precursors, using

- improved forward emission modelling for the Biogenic Volatile Organic compounds (BVOCs)
- inverse modelling of emissions based on a global CTM

2/ the degradation mechanism of monoterpenes (an important class of BVOCs), focussing on their oxidation by the hydroxyl radical (OH), based on

- experimental (fast-flow reactor) studies
- a theoretical investigation of their oxidation mechanism
- model simulation of their oxidation in laboratory or atmospheric conditions, including the formation of secondary organic aerosol (SOA)

3/ the chemistry and impact of selected non-methane volatile organic compounds (NMVOCs) in the upper troposphere and lower stratosphere (UT/LS), based on

- experimental, theoretical and modelling investigations of selected reactions of organics in the temperature and pressure regime typical of this region of the atmosphere

---

[1] http://www.unfccc.de/

4/ the future evolution of the global tropospheric composition, through contributions to international (IPCC) modelling exercises (IPCC-TAR report, IPCC-ACCENT modelling experiments)

The importance of BVOCs stems from their large emissions at the global scale. Their chemical degradation in the atmosphere has a strong impact on the oxidizing capacity of the atmosphere, because of their multiple influences on the budgets of O_3 and OH radicals. In addition, the degradation of BVOCs leads to the formation of semi-volatile (carbonyl and carboxyl) compounds, which are considered to be a major source of secondary organic aerosols (SOA).

Isoprene and monoterpenes are the most prominent classes of BVOCs. The emissions and chemistry of isoprene and, in some cases, α-pinene (as representative for the monoterpenes) are now included in many tropospheric CTMs. The emissions rates in these models are calculated as simple functions of temperature, light, and ecosystem type, following the model developed by Guenther *et al.* (1995). The large uncertainty in the global emission estimates (about a factor 3) requires a dedicated effort to improve the representation of the canopy processes involved (e.g. radiative transfer, calculation of leaf temperature), and to validate the emission algorithms by careful comparisons with campaign data. Another approach, also explored in this project, consists in the derivation of improved emission estimates by inverse modelling. Following this methodology, the emissions are constrained by requiring that the CTM-calculated distribution of known BVOC by-products (e.g. CO) matches a representative set of observations.

Whereas the chemistry of isoprene is well documented, the degradation of monoterpenes is still highly uncertain. While a wide variety of oxidation products have been observed in both the gas- and particulate phases, their yields show a large uncertainty range. These yields are expected to be strongly dependent on photochemical conditions (e.g. radiation, NO, NO_2, O_3, etc.). These conditions are unfortunately not well controlled in most experimental set-ups; of particular importance are the respective contributions of O_3, OH and NO_3 to the overall monoterpene sink and the formation of aerosols leading to poor overall carbon balances. For these reasons, many laboratory results cannot be properly interpreted, unless thorough modelling studies are conducted to reproduce the experimental conditions. In particular, advanced tools are required in order to better quantify the partitioning of the low-volatility products between the gas and aerosol phases. The methods proposed in this project to reduce the uncertainties on the oxidation of monoterpenes include

- fast-flow reactor investigations of the reaction of selected monoterpenes with OH, in the presence of NO and at reactor pressures of 50-200 Torr

- detailed theoretical investigation of the oxidation of two monoterpenes by OH in the presence of NO, and construction of a semi-explicit oxidation mechanism for α-pinene, the most abundant monoterpene
- simulation of laboratory experiments for the oxidation of α-pinene by OH with and without NO, based on the mechanism mentioned above
- derivation of a reduced α-pinene oxidation mechanism for use in a global CTM, and assessment of its impact in the troposphere

The uncertainties regarding oxidant production in the UT/LS are still very large. Recent reports have indicated (i) that the chemistry of carbonyls is highly relevant in this area, in particular with respect to the production of odd hydrogen (HO_x) radicals, and (ii) that this chemistry requires new experimental and theoretical studies, because the degradation processes of these compounds at the low temperatures and pressures of the UT might be different from their boundary layer chemistry. Acetone, frequently present in the UT/LS at ppb-levels, is known to be a major source of HO_x radicals, by direct photolysis as well as by photolysis of CH_2O formed in its OH-initiated oxidation. Very recent measurements have indicated that this reaction with OH at 200-220 K does not proceed only by H-abstraction, but also by a mechanism resulting in acetic acid (Wollenhaupt and Crowley, 2000; Vasvary et al., 2001). It has likewise been reported that the reaction of acetaldehyde with OH yields mainly formic acid (Taylor et al., 1996) rather than acetyl, the known precursor of PAN. The low-temperature chemistry of acetic acid is not yet established, but there is a possibility that its OH-initiated oxidation yields products which photodissociate rapidly, making also acetic acid an important HO_x source. In addition, the evidence for association reactions of HO_2 with formaldehyde and acetaldehyde (Veyret et al 1989; Tomas et al., 2001) prompts us to explore the possibility of HO_2-initiated oxidation mechanisms of aldehydes as well as ketones at the very low temperatures of the tropopause region, even though HO_2 + ketone reactions are generally accepted to be negligibly slow in all conditions (Gierczak and Ravishankara, 2000). The specific studies proposed in this project to (re)evaluate the role of oxygenated NMVOCs in the UT/LS include:

- experimental determinations of the primary-product distributions of the OH reactions with acetaldehyde, propionaldehyde, acetone, and acetic acid
- detailed theoretical investigations of the mechanisms of the OH and HO_2 radical reactions with $C_1 - C_3$ carbonyl and carboxyl compounds and of the role thereby of H-bonded pre-reactive complexes
- 3-dimensional modelling studies to assess the potential global impact of HO_2- initiated removal of carbonyls near the tropopause

2. METHODS

2.1 EMISSION MODELING

2.1.1 Development of a vegetation canopy model

MOHYCAN, a multi-layer vegetation canopy model, has been developed in this project. The emissions of Biogenic Volatile Organic Compounds (BVOCs) are known to depend on leaf temperature and visible radiation. Following Goudriaan and van Laar (1994), the model determines the vertical profile of visible and infrared radiation in the canopy, including their direct and diffuse components. The radiative calculations have been validated against observations, and compared with the results of a simple model. Leaf temperature is also calculated in each layer, for shaded and sunlit leaves. Stomatal resistance is parameterized according to the model of Sellers *et al.* (1986). Water stress is found to play a significant role in the determination of the emissions, with high stresses leading to smaller stomatal resistance and generally to higher temperatures and larger emissions.

2.1.2 Inverse modelling of emissions in a global CTM

Inverse modelling is a new and promising approach for constraining the emissions of tropospheric compounds. It assumes that errors in the emission inventories are the main cause for biases between the distributions predicted by a CTM and the observations. Inverse modelling consists in the optimization of the CTM emissions by the minimization of the model/data bias. This approach has been successfully applied in past studies to inert and weakly reactive gases like CO_2 and CH_4.

In a first step in this project, and in collaboration with the Service d'Aéronomie in Paris, the direct emissions of carbon monoxide (CO) have been optimized in the CTM IMAGES (Müller and Brasseur, 1995), based on network (CMDL) observations of this compound. It was assumed that the concentrations of CO respond in a weakly non-linear way to changes in the emissions, a hypothesis not always verified in the general case. The emission parameters which were optimized are the aggregated emissions from the main categories (anthropogenic, biomass burning, oceans …) over large regions (Europe, Asia, etc.). Although the emissions of BVOC represent a large source of CO in the atmosphere, this source was not optimized in this study.

In a second step, a new methodology has been developed for inverting the emissions, which allows non-linearities. It is based on the 'adjoint' model method also used in 4DVar meteorological assimilation. The emissions of CO, NO_x and BVOC have been simultaneously optimized following this method, based on network CO measurements and satellite-derived NO_2 vertical abundances.

In a third step, the inversion methodology has been further refined to allow for 'grid-based' inversions, where the emissions from every model grid cell are optimized (instead of their average value over large regions), thereby reducing the aggregation error resulting from their assumed geographical and seasonal distribution within the large regions. In principle, this powerful new tool should allow an optimal exploitaton of satellite data which, in contrast to in-situ measurements, provide a broad spatial coverage. This approach is now being tested with the CO global fields from the MOPITT instrument.

2.2 LABORATORY STUDY OF MONOTERPENE-OH REACTIONS (Chris Vinckier, Katholieke Universiteit Leuven)

2.2.1 Experimental set-up

In order to investigate the chemistry of important terpenes (α- and β-pinene, Δ^3-carene and limonene), a fast-flow reactor system has been built, and an appropriate sampling method has been developed for the oxidation products. In this system, hydroxyl radicals are generated by the reaction $H + NO_2 \rightarrow OH + NO$. A major advantage of the fast-flow reactor technique is the absence of ozone in the system. Ozone represents a serious difficulty in photochemical reactors, due to the interference of ozone reactions with organics during sampling and analysis.

A major challenge in laboratory studies dedicated to the oxidation of terpenes is the identification and quantification of the semi-volatile products, in particular, mono- and di-ketones, aldehydes and carboxylic acids. Besides methods based on Fourier transform infra red (FTIR) (Nozière *et al.*, 1999) and proton transfer reaction mass spectrometry (PTR-MS) (Wisthaler *et al.*, 2001), high-performance liquid chromatographic (HPLC) separation techniques with UV-VIS diode-array or mass spectrometric detection have been applied (Van den Bergh *et al.*, 2000). In addition, a widely used procedure for monitoring carbonyl compounds in air is based on their derivatization with 2,4-dinitrophenylhydrazine leading to 2,4-dinitrophenylhydrazon (DNPH) (Purdue *et al.*, 1991; EMEP, 1996). Due to the presence of isomers and

dicarbonyls, HPLC with UV-VIS is inadequate for monoterpene oxidation products. New detection methods have been developed in this project, which overcome these limitations.

The semi-volatile reaction products are collected on a liquid nitrogen trap coated with the DNPH reagent and an internal standard, benzaldehyde-DNPH, a choice motivated by the fact that benzaldehyde cannot be formed from the terpene compounds used here, as verified in blank experiments. The use of a cold trap strongly improves the detection capability, although it requires an additional internal standard to correct for product losses.

Sampling and derivatization are well separated using this procedure, which allows a better control of the reaction conditions (Levart and Veber, 2001). Derivatization significantly improves the detection limits. Only carbonyls can be detected, but since these compounds are generally formed as primary products in oxidation reactions, this method is suited for analysis of the terpene-OH reactions. The procedure for the derivatization and detection of carbonyl compounds is amply described in the literature (e.g Grosjean *et al.*, 1999; Kölliker *et al.*, 1998).

2.2.2 Analytical techniques

The GC-MS technique is used for structure determination and purity control of synthesized products (Van den Bergh *et al.*, 2000). Having verified that HPLC-DAD generates very reproducible results for mono-carbonyls, this technique is adopted for quantification of reaction products. Although it is highly suited for quantitative analysis, it has only a poor identification capacity.

HPLC-MS is mainly used for the identification of unknown compounds. The ability of recording fragmentation spectra of unknown compounds allows an unambiguous determination of the compound's structure. It is a very valuable technique for detecting and quantifying multifunctional organic compounds (e.g. dicarbonyl compounds such as caronaldehyde). For determining product yields, the reproducibility of HPLC-MS is lower than for HPLC-DAD.

Sample analysis is performed with a mass spectrometer equipped with Atmospheric Pressure Chemical Ionization (APCI) during the first stage of the project (Van den Bergh *et al.*, 2000). In a later stage, new analytical methods have been elaborated due to the availability of a new LC-MS apparatus containing an Ion Trap mass

analyzer and the new ESI (electro-spray ionization) ionization technique. The mass spectrometer is equipped with an ESI and an APCI source, both of which are soft ionization technique causing minor fragmentation (De Hoffman and Stroobant, 2003). For the detection of DNPH derivatives both ionization methods are used in the negative mode.

2.2.3 Synthesis

Several compounds have been synthesized and purified for calibrating the instruments, as summarized in Table I.

Table I: Overview of synthesized compounds.

Reaction	Compounds	DNPH derivatives
β-pinene - OH	Myrtanal, trans-3-hydroxynopinone	Nopinon-DNPH, Perillaldehyde-DNPH, Myrtanal-DNPH, trans-3-Hydroxynopinone-DNPH
Δ^3-carene - OH	Caronaldehyde	Caronaldehyde-DNPH, Caronaldehyde-di-DNPH
limonene-OH	Endolim, 4-AMCH	Endolim-di-DNPH, Endolim-DNPH, 4-AMCH-DNPH

Endolim and caronaldehyde are synthesized through the controlled ozonolysis of the original terpene. Trans-hydroxynopinone is synthesized by the ozonolysis of trans-pinocarveol. The derivatives are synthesized as in Behforouz *et al.* (1985). All synthesized compounds have been checked for impurities with GC-MS.

2.2.4 Analysis method

An extensive analytical study has been carried out on the quantitative detection of terpene degradation products. Analysis capabilities are investigated using both APCI and ESI ionization techniques, in the positive and negative mode. In addition, different detection modes (full-MS, SIM (Single Ion Monitoring), MS-MS) have been evaluated.

Qualitative analysis

The chromatogram obtained in full MS mode is used to split the total analysis time in different segments, each segment corresponding to a different derivative. Further information on the parent ion can be obtained from the MS-MS spectra generated by its collision-induced decomposition. As voltage amplitude increases in the ion trap, a resonance excitation process leads to the soft fragmentation of the parent ion. Isolation width and collision energy is optimized for each individual parent ion.

Quantitative analysis

The reproducibility of the HPLC-MS technique as well as its detection limits have been determined for both the APCI (-) as ESI (-) ionization mode and both the SIM as MS-MS scan mode. The results have been validated against those of the HPLC-DAD technique. Several instrumental settings related to ionization are optimized manually, e.g. the APCI vaporizer temperature and the capillary temperature. The other parameters are optimized by the auto-tune program of the instrument.

Calibration curves for the DNPH derivatives are constructed by plotting the area ratio of the compound of interest and the internal standard against their concentration ratio in the standard solution. Eight standard solutions with concentrations between 100 and 3000 ppb have been analyzed. Limits of detection are calculated in accordance with the German Institute of Standardization (1994).

Both ESI and APCI in the negative mode are found to be suitable for the quantitative analysis of mono-DNPH derivatives. ESI (-) in combination with SIM shows the lowest detection limits. In addition, ESI shows also a better reproducibility than APCI. Detection of di-carbonyl compounds can be performed only by APCI (-) with a somewhat lesser sensitivity than HPLC-DAD. Moreover, better results are obtained in the SIM mode than in MS-MS mode.

2.3 LABORATORY STUDY OF VOC-OH REACTIONS (E.A., BRUSSELS)

2.3.1 Instrument description

A new instrument, which consists of a quartz fast flow reactor (FFR) coupled to a low pressure (0.8 Torr) chemical ionization mass spectrometer (CIMS), has been built in order to detect and quantify some of the oxidation products of the reactions of OH radicals with acetone and monoterpenes. As in the study conducted by the team C. Vinckier in KULeuven (Sect. 2.2.1), OH radicals are generated by the reaction of NO_2 with H atoms produced by the dissociation of H_2 in a microwave discharge. The reactant is introduced in the reactor through a moveable injector which ends on a Teflon diffuser to promote mixing.

Reactants and products are sampled at the downstream end of the reactor and detected in the CIMS, which is a stainless steel flowing afterglow reactor coupled to a quadrupole mass spectrometer (Amelynck *et al.*, 2000). Detection is performed by using appropriate ion/molecule reactions which result in specific product ions which are 'fingerprints' of the molecules to be detected. The precursor ions are produced by reaction of electrons and Ar^+ ions with H_2O or electronegative gases. The use of helium as bath gas in both FFR and CIMS resulted in a good mixing in the CIMS and made absolute and accurate CIMS-based quantification possible, as demonstrated in calibration experiments with acetone and α-pinene.

In the course of the project the FFR has been replaced by a triple-nested high pressure turbulent flow reactor (HPTFR), similar to the one at LCSR-Orléans (Kujui *et al.*, 2003). Its major advantages are an efficient mixing in turbulent conditions, a better control of OH losses and the possibility to perform experiments in nitrogen buffer gas at higher pressures (200 Torr). Hydroxyl radicals are made in the outer injector by the reaction of NO_2 with H radicals produced in the inner injector in a microwave cavity. Reactants are introduced upstream the outer injector. By translating the outer injector, the OH/VOC reaction time can be varied. To enhance the dynamic range of the CIMS detection system, its flow tube is equipped with a filament ion source operated in Ar buffer gas and the reaction zone has been shortened. A drawback of the use of Ar and N_2 is a less efficient mixing in the CIMS resulting in a less accurate quantification of the VOCs and their oxidation products. This quantification therefore requires careful calibration measurements.

2.3.2. Methods of analysis

The yield of an oxidation product (OP) is defined as the ratio of its concentration [OP] to the reactant concentration change (Δ[VOC]):

Y_{OP} = [OP]/ Δ[VOC].

Since the VOC and OP concentrations in the CIMS are about 1000 times lower than in the neutral reactor, neutral chemistry is stopped in the CIMS, and the ratio [OP]/Δ[VOC] is unchanged in the CIMS.

Absolute and accurate CIMS-based quantification requires the knowledge of the rate constants *k* and product distributions *f* of the relevant ion/molecule reactions, and of a set of instrumental parameters (the ion residence time *t* in the reaction zone, mass discrimination of the CIMS detection part). The ion/molecule reaction parameters have been measured in a selected ion flow tube instrument (SIFT) (Sect. 2.3.3 and 3.3.1). Mass discrimination factors *MDF* and ion residence time *t* have been determined in the CIMS. Differential diffusion of precursor and product ions is taken into account through the use of calculated diffusion enhancement factors (DE) (Španěl *et al.*, 2001), and turned out to be an extremely important factor.

For a species R detected by means of the positive ion/molecule reaction $H_3O^+ + R \rightarrow Y^+ + P$, the reactant concentration [R] is given by:

$$[R] = \frac{1}{kf(Y^+)t} \times \frac{[Y^+]}{[H_3O^+]} \times MDF(Y^+) \times DE(Y^+, t)$$

In the OH/α-pinene experiments, carried out in the FFR/CIMS instrument, acetone, formaldehyde and α-pinene are quantified as described above. The ion/molecule reaction parameters have been either measured in the SIFT (see Sect. 3.3.1) or found in the literature (Španěl *et al.*, 1997).

Detection of acetic acid as a possible reaction product of OH with acetone was also carried out in the FFR/CIMS apparatus using CF_3O^- and SF_6^- precursor ions which both react with acetic acid through fluoride transfer (Amelynck *et al.*, 2000).

For the OH/β-pinene experiments, performed in the HPTFR/CIMS apparatus, acetone, nopinone and β-pinene 'fingerprint' ion signals using H_3O^+ as well as NO^+

CIMS precursor ions have been calibrated by introducing controlled flows of these species into the HPTFR.

2.3.3 Study of ion/molecule reactions in support of the CIMS detection of VOCs and their oxidation products

The SIFT apparatus consists of an ion source, a part which selects the appropriate source ion, a reaction zone (flow tube) where the reactant gas is introduced, and a detection/analyzing part.

A variety of ions, produced by a microwave discharge in an air/water vapour mixture, are electrostatically extracted from the discharge into the selection part of the SIFT apparatus, which consists of two differentially pumped chambers. The first chamber contains several ion lenses, the second chamber houses a quadrupole, which selects the appropriate source ion (in our case H_3O^+, NO^+ or O_2^+). The mass selected source ions are injected into the reaction zone through a Venturi inlet system (Adams and Smith, 1976), where they are convectively transported by a helium carrier gas flow towards the detection quadrupole, followed by an electron multiplier. Three gas inlets are foreseen in the reaction zone: two for the introduction of the reactant gas (reaction rate constant and product ion distribution measurements) and one for the determination of mass discrimination effects of the detection part. Typical pressure in the reaction zone is 1.5 mbar.

The ion/molecule reaction rate constant k is derived from the decay $\ln(I/I_0) = -k\tau[X]$ of the source ion signal I versus the neutral reactant concentration $[X]$. The residence time τ of the ions in the flow tube is measured separately. The reaction rate constants of H_3O^+ with the different reactants are derived in an absolute way: the concentration of the reactant neutral $[X]$ is varied by introducing into the flow tube different flows of a known volumetric mixture of the reactant in helium, prepared in volume calibrated glass containers.

For the low-volatility reactants pinonaldehyde (PIN) and caronaldehyde (CAR), the method described above cannot be used. Therefore, a known amount of liquid PIN (CAR) is put in a small weighing boat in a cylindrical glass container filled with helium and heated up to 360 K in a furnace. By choosing the amount of PIN (CAR) in such a way that the pressure is lower than the vapour pressure [Hallquist *et al.*, 1997], we can assume that PIN (CAR) in the cylinder is in the gas phase and the dilution of the reactant can be interfered.

The reaction rate constants of NO^+ and O_2^+ with the different compounds are measured in a relative way with respect to the one of H_3O^+ by injecting the three precursor ions simultaneously and by recording their signal as a function of the reactant concentration. The same reactant gas inlet methods are used as for the absolute measurements.

To determine product ion distributions, a removable gas inlet is used, located in front of the inlet plate of the analyzing quadrupole to minimize diffusion enhancement. Volumetric mixtures of the reactant in glass bottles are used, or the reactant is introduced by blowing helium over the liquid reactant. Mass discrimination by the analyzing quadrupole and electron multiplier is taken into account (Španěl *et al.*, 2001).

All reactants except PIN, CAR and glyoxal are commercially available. PIN and CAR are synthesized by monoterpene ozonolysis (Vinckier *et al.*, 1997, Rautenstrauch *et al.*, 1984). Glyoxal is prepared from the hydrated trimer $C_6H_6O_6.2H_2O$ (Horowitz *et al.*, 2001).

2.4   THEORETICAL STUDY OF THE OH-INITIATED OXIDATION OF MONOTERPENES AND CONSTRUCTION OF EXPLICIT MECHANISMS (J.P.)

We took up the major challenge of developing detailed chemical mechanisms for the OH-initiated oxidation of α-pinene, pinonaldehyde and β-pinene under realistic atmospheric conditions (with NO_x present), *on the exclusive basis of objective chemical-kinetics knowledge and validated quantitative structure-activity relationships (SARs), and/or from first principles*, i.e. quantum-chemical potential energy profiles (PES) and associated parameters in combination with advanced statistical rate theories.

2.4.1 Quantitative Structure-Activity Relationships and their Development

For this demanding task (begun in 1997), extensive use was made of validated quantitative structure-activity relationships as prime mechanism-construction tools. The SARs employed in this work concern: the initial reactions of OH with the polyalkene; the branching of the reactions of the subsequent peroxy radicals with NO; and the reactions of the resulting (substituted) alkoxy radicals:

(i)   The site-specific SAR for addition of OH to (poly-)alkenes developed earlier by us (Peeters et al., 1994 and 1996). This SAR, of major importance for this project, provides the rates of the individual OH-addition channels.

(ii)   A mini-SAR for H-atom abstraction from (biogenic) poly-alkenes, complemented by specific radical stabilisation effects for bicyclic terpenic structures, developed in this project; for the sake of brevity, we refer in this respect to the pertaining publications:

> - L. Vereecken, J. Peeters, H-Atom Abstraction by OH-Radicals from (Biogenic) Poly-Alkenes: C-H Bond Strengths and Abstraction Rates, Chem. Phys. Lett., 333, 162-168, 2001

> - L. Vereecken, J. Peeters, Enhanced H-atom abstraction from pinonaldehyde, pinonic acid, pinic acid and related compounds : theoretical study of the C-H bond strengths, Phys. Chem. Chem. Phys., 4, 467-472, 2002

(iii)   The recently upgraded SAR of Arey et al (2001) for the branching fractions of organic nitrate formation versus alkoxy + NO_2 production in reactions of alkylperoxy radicals with NO.

(iv)   A general SAR for the activation energy E of isomerization of substituted alkoxy radicals by strain-free 1,5-H shifts; we derived this SAR from the available literature data (Atkinson et al. 1999):

> $E(1,5\text{-}H) / (kcal/mol) = 8.4 - 0.65 \times (99.5\ kcal/mol - D_{C\text{-}H})$,

where $D_{C\text{-}H}$ is the bond dissociation energy of the migrating H-atom. The SAR is supported by the theoretical study of the 1-butoxy case in this project; again for the sake of brevity, we refer here to the pertaining publication:

> - L. Vereecken, J. Peeters, The 1,5-H-shift in 1-butoxy: a case study in the rigorous implementation of Transition State Theory for multi-rotamer systems, J. Chem. Phys., 119, 5159-5170, 2003

(v)   A generalised SAR for the barriers to decomposition of substituted alkoxy radicals, developed in this work (Peeters et al., 2004); see RESULTS, *sub* 3.4.

The fate of oxy radicals is of pivotal importance in the oxidation mechanisms of complex VOCs. In general, oxy radicals may undergo possibly competing β C—C scissions, 1,5-H migrations (isomerisations), and reaction with O_2. Whereas the reactions with O_2 all have rates (Atkinson et al. 1999) of $(4\text{-}5) \times 10^4$ s^{-1} in ambient conditions, the rates of the dissociation and isomerisation reactions can range from

<1 s^{-1} to 10^{12} s^{-1}, depending on the barrier height and rigidity of the transition structure. As a result, for large oxy radicals, one particular reaction will often dominate. Given its major importance to this project, the development of the oxy decomposition SAR (v) will be described in the RESULTS section 3.4.

2.4.2 Quantum Chemical and Statistical-Kinetics methods

For reactions that could not be quantitatively described (with sufficient reliability) by SARs, as well as for chemically activated reactions occurring in the mechanisms, the kinetics and product makeup were predicted by advanced theoretical methods. Potential energy and rotation-vibration data were computed at various levels of ab initio and DFT theory, ranging from B3LYP-DFT/6-31G(d,p) to B3LYP-DFT/6-311+G(2df,2pd), in some cases complemented by CC single point energies at the CCSD(T)6-311+G(2d,p) level. For several structures, including systems with intramolecular H-bonding, a large number of (rotameric) conformers had to be taken into account. Rate coefficients of thermal reactions were subsequently computed using multi-conformer transition state theory (MC-TST), whereas for chemically activated multichannel processes, the (pressure-dependent) rates and product distributions were obtained using weak-collision RRKM theory and master-equation analysis, as implemented in our URESAM programme suite (Vereecken et al. 1997). Note that the B3LYP-DFT/6-31G(d,p) level of theory has been validated earlier for oxy radical decompositions (Vereecken and Peeters, 1999; Vereecken et al. 1999), for which DFT results differed on average only 0.5 - 1 kcal/mol from high-level ab initio calculations and from experimental barrier heights. This was later confirmed also for 1,5-H shifts in oxy radicals (Vereecken and Peeters, 2004).

2.5   A MODEL FOR THE OXIDATION OF ALPHA-PINENE

2.5.1 Gas-phase oxidation of α-pinene

The semi-explicit mechanism for the oxidation of α-pinene and pinonaldehyde by OH developed by the team of J. Peeters at KULeuven (Sect. 2.4) has been implemented in a numerical 'box' model. The further reactions of the products are parameterized. A simple ozonolysis mechanism is also included. The numerical model (Damian-Iordache *et al.*, 1995) solves the continuity equation for the ~600 species involved in the mechanism, given a set of initial conditions.

The kinetic rates used in the model are based on previous studies. Due to the large number of compounds involved in the mechanism, a special treatment is required for the permutation reactions of peroxy radicals, since their explicit representation would be too demanding in terms of implementation and computational time. The peroxy radicals are grouped into structural classes. Each class is characterized by a self-reaction rate determined from a review of literature data. The permutation reactions of a specific radical are represented as the reactions of this compound with the different classes. The cross-reaction rates are calculated as twice the geometric average of the self-reaction rates of the reacting compounds.

The photolytic parameters (cross sections and quantum yields) for the photolysis reactions implied by the mechanism are determined from a review of the available data for the photolysis of organic compounds. The actinic fluxes are determined from either a detailed radiative transfer model accounting for light absorption, scattering and reflection (for atmospheric conditions), or from the measured photolysis frequency of a reference compound (for laboratory conditions).

2.5.2 Gas/aerosol partitioning

The gas/particle partitioning of organic compounds is generally estimated from their saturation vapour pressures (Pankow, 1994). Given the lack of data for the vapour pressures of α-pinene oxidation products, a new estimation method has been developed in this work. It relates the vapour pressure of an oxygenated compound to the vapour pressure of its parent alkanoic compound (generally well known from the measurements) and to the number and types of chemical functionalities present in the molecule. The method accounts for the effect of substitutions on the carbon bearing an alcohol or nitrate function. The adjustable parameters in the method are determined by minimizing the bias between the model and a large set (~100) of measurements. The comparison of our results with a widely used prediction method (UNIFAC) indicates a better overall performance of our method, especially for dicarbonyls and diols. Large discrepancies are found in the comparison of our results with previous studies for specific compounds, like pinic acid, pinonaldehyde and the hydroperoxides, but they are generally well understood from an examination of the methods assumptions.

Since multifunctional carboxylic acids (e.g. pinic acid) can be expected to be mostly present as dimers in laboratory conditions (Hoffman *et al.*, 1998), we propose that the partial vapour pressure of the pinic acid dimer should be close to the

experimental sub cooled vapour pressure for pinic acid ($\sim 10^{-6}$ Torr). Dimerization is included in the mechanism for pinic acid and pinonic acid, using preliminary estimates of the kinetic rates provided by the team of J. Peeters in Leuven.

2.5.3 Reduced mechanism (J.-F.M.)

The explicit α-pinene mechanism of ~600 species and ~2000 reactions has been reduced to a set of 30 species and ~100 reactions, suitable for use in a 3D model. To achieve this, two intermediate mechanisms have been first designed, for NOx-free and for high-NO (~1 ppm) conditions. These are obtained by merging oxidation channels producing peroxy radicals of similar structures and by using surrogates for the products showing similar structures and reactivities towards ozone and OH. The peroxy radicals produced in the first oxidation steps are considered explicitly. The other peroxy radicals are represented by two generic peroxy radicals. Their yields are adjusted according to the yields obtained with the explicit mechanism for the corresponding chemical conditions.

Comparisons between the reduced and the detailed mechanism show a very good agreement for both the gas and aerosol phases. Sensitivity tests show that the reduced mechanism reproduces very well the explicit mechanism for the most common range of atmospheric NO (10-100 ppt).

2.6 STUDIES OF OH AND HO$_2$ REACTIONS OF IMPORTANT OXYGENATED ORGANICS IN THE UT/LS

2.6.1 Experimental techniques (team of **J. P**., KULeuven)

The primary reaction products and the mechanisms of the elementary reactions of OH radicals with acetaldehyde, propionaldehyde, acetone and acetic acid were investigated experimentally using the discharge-flow technique coupled to molecular beam sampling mass spectrometry (DF – MBMS). Hydroxyl radicals were generated in known amounts by the H + NO$_2$ $\rightarrow$ OH + NO titration reaction, with the H atoms generated upstream in a microwave discharge. The MBMS-sensitivity to the reactants and (potential) molecular reaction products (H$_2$O, formic and acetic acid, CO$_2$ …) were determined separately by feeding known flows into the reactor.

2.6.2 Theoretical methodologies (**J. P**.)

The experimental observations were supported/complemented by quantum chemical and theoretical-kinetic calculations in order to determine the reaction mechanisms and predict rate coefficients and their temperature dependence.

Relevant potential energy profiles (PES) and vibration/geometric parameters were calculated at appropriate levels of DFT and *ab initio* quantum theories, *viz.* the B3LYP-DFT/6-31G(d,p) and B3LYP-DFT/6-311++G(d,p) methods with single-point CCSD(T)/6-311++G(2d,2p) energy calculations for the acetone + OH reaction, and the B3LYP-DFT/6-311++G(2df,2pd) method with single point energies at a modified G2M(CC,MP2) level for the acetic acid + OH reaction. For the newly explored reactions of HO_2 radicals with carbonyl compounds (acetone, formaldehyde, etc.), the state-of-the-art *ab initio* methods G3, CBS-QB3 and a nearly-converged G2M//DFT variant were brought to bear for optimal accuracy; these three high levels of theory were found to give quasi-identical results.

Reaction rates were calculated using advanced statistical rate theories: multi-conformer Transition State Theory for thermal processes and multi-conformer RRKM theory combined with weak-collision master equation analyses for chemically activated reactions, including reactions proceeding through H-bonded complexes.

3. RESULTS AND DISCUSSION

3.1 BVOC EMISSION MODELING

3.1.1 Comparison with field observations

The confrontation of the emission model (Sect. 2.1.1) with flux measurements at mid- and Tropical latitudes shows marked differences between the performance of the algorithm at different sites or at different times of the year. The model/data bias does generally not exceed a factor of 2, except at an Amazonian site, where the model values are overestimated by almost an order of magnitude. The figure below shows the measured and modelled isoprene fluxes (daily averages) at a mid-latitude forest site. The model values are scaled to the average estimated from the data. The model succeeds in reproducing the day-to-day variation in the emissions. The overestimation in spring and fall is probably an effect of leaf age. This would confirm that this parameter should be considered in BVOC emission algorithms, as is the case in the new MEGAN model (Guenther *et al.*, 2005).
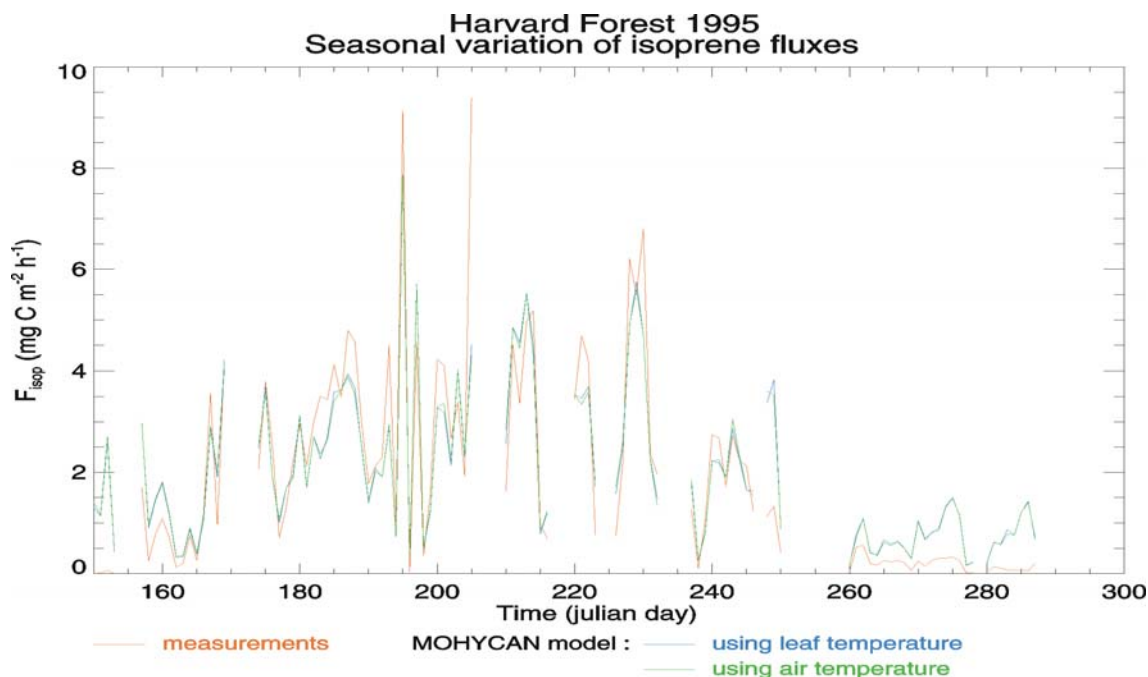

Figure 1: Measured (orange curve) and calculated (green and blue) daily averaged isoprene fluxes at a mid-latitude forest site between June and October 1995.

3.1.2 Global BVOC emissions

The MOHYCAN model has been used to estimate the global emissions of BVOCs at a resolution of 0.5°, based on a choice of several datasets for the distribution of vegetation properties (Leaf Area Index) and meteorological parameters (chiefly solar downward radiation and air temperature). The ecosystem distribution and their associated BVOC emission properties (emission rates in standard conditions) are as in Guenther *et al.* (1995), which allows a comparison of our results with the widely used inventory described in this study. Our best estimate for the global emissions is 620 Tg/year for isoprene and 126 Tg/year for the monoterpenes. The impact of our calculation of leaf temperature (assumed to be identical to air temperature in Guenther *et al.*) is illustrated by Figure 2. A positive difference between leaf and air temperature (left panel) of 1-3 degrees Celsius is predicted in dry/warm areas, e.g. in the dry season at subtropical latitudes. This leads to an increase of 10-40% in the calculated isoprene emissions in these regions (right panel).
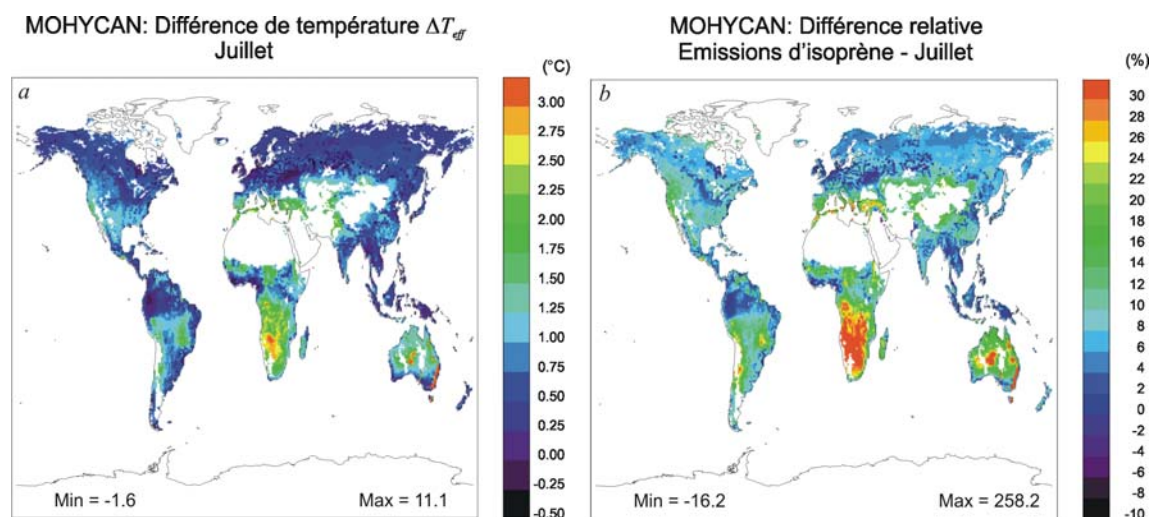

Figure 2: Left panel: calculated difference between leaf and air temperature in July. Right panel: Change in isoprene emissions (%) resulting from this difference.

3.2 LABORATORY STUDY OF MONOTERPENE-OH REACTIONS (C.V., LEUVEN)

3.2.1 β-pinene + OH

Identification of products

The β-pinene/OH reaction is found to produce formaldehyde, acetaldehyde, acetone, trans-3-hydroxynopinone, nopinone, perilla alcohol, perillaldehyde and myrtanal. Formaldehyde and nopinone are the most important oxidation products, as previously determined by other research groups. Plausible formation mechanisms for these compounds can easily be proposed, except for acetaldehyde and trans-hydroxynopinone.

Product yields

The average relative molar yields of formaldehyde, acetone and nopinone have been determined at 50 and 100 Torr, as seen in Table II. By definition, the relative yields add up to 100%. Caution is required when comparing these results with true (absolute) yields from other studies, since many products might be undetected. Note that changing the reaction time between 42 and 108 ms is found to have little or no effect (a few percent) on the yields.

Table II: Relative yields (mol %) for β-pinene/OH reaction products at 50 and 100 Torr, [β-$C_{10}H_{16}$] ~ $5x10^{12}$ molecules/cm^3, [H_2] = $1.37x10^{13}$ molecules/cm^3, [NO_2] = $3.62x10^{12}$ molec/cm^3, [O_2] = $3.24x10^{17}$ molec/cm^3 (50 Torr), [O_2] = $6.48x10^{17}$ molecules/cm^3 (100 Torr), reaction time = 42 ms.

Reactor pressure (Torr)	50	100
Formaldehyde	48 ± 2	43 ± 2
Acetaldehyde	1.2 ± 0.6	0.6 ± 0.4
Acetone	20 ± 3	7.8 ± 0.5
Nopinone	31 ± 1	49 ± 2

At 50 Torr, formaldehyde is the dominant product while at 100 Torr, nopinone represents almost 50% of the observed products. The yields reported in previous studies for formaldehyde, $54 \pm 5\%$ (Hatakeyama *et al.*, 1991) and $45 \pm 8\%$ (Orlando

et al., 2000) are close to our values. For nopinone, the measured product yields of 27 ± 4% (Hakola *et al.*, 1994) and 30 ± 4% (Arey *et al.*, 1990) are somewhat lower than in our data, in particular at 100 Torr. A major discrepancy with other literature data is seen for acetone with a yield of 2±2% (Orlando *et al.*, 2000), at least a factor of 3 lower than our value. This might be partly explained by an effect of pressure on the yields, as indicated by the sharp decrease of our acetone yields between 50 and 100 Torr. However, in recent work using the PTR-MS technique, a primary acetone yield of 13 ± 2 % has been seen (Wisthaler *et al.*, 2001). Larsen *et al.* (2001) also reported a large acetone yield of 11 ± 2%, but their yield of formaldehyde of 23 ± 2% is much lower than that in our work.

Influence of NO

The effect of changes in NO concentration on the product distribution is displayed in Figure 3. The NO concentration in the reactor is varied between $2.2 \; 10^{12}$ and $2.2 \; 10^{13}$ molec/cm^3 by the introduction of additional NO through the NO$_2$ inlet.

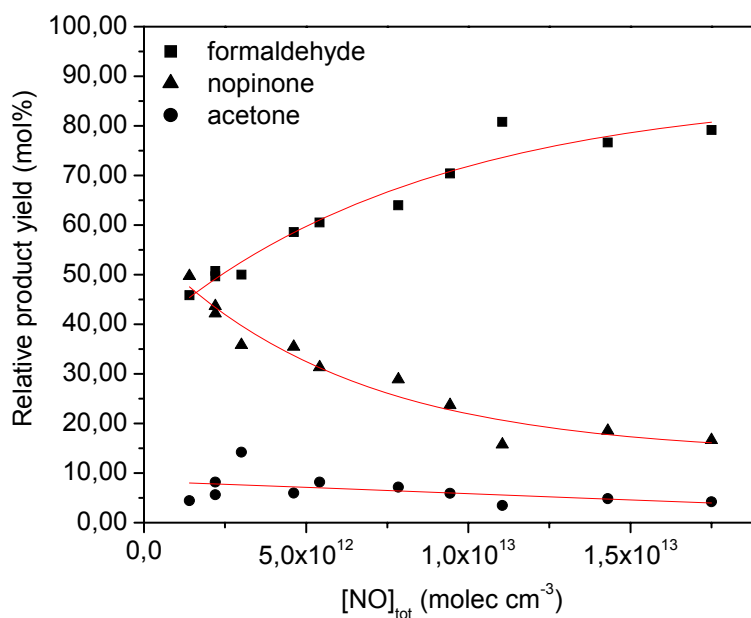**Figure 3**: Average yields of formaldehyde, acetone and nopinone (mol %) as a function of NO concentration at 100 Torr, [β-C$_{10}$H$_{16}$] = 5 10^{12} molec/cm^3, [H$_2$] = 1.37 10^{13} molec/cm^3, [NO$_2$] = 1.4 – 2.8 10^{12} molec/cm^3, [O$_2$] = 6.48 10^{17} molec/cm^3, [NO] = 0.8 – 16.7 10^{12} molec/cm^3, reaction time = 42 ms.

As seen on this figure, the yield of nopinone decreases with [NO], at the expense of formaldehyde. At the highest NO concentration, the nopinone yield is reduced by a factor of more than 2, while the formaldehyde yield is almost doubled. The yield of acetone decreases only slightly with [NO]. These observations differ from those obtained earlier for the α-pinene/OH reaction, where no pronounced effect of NO was observed.

3.2.2 Δ^3-carene + OH

Identification of products

The most important reaction product of the Δ^3-carene oxidation is found to be the di-carbonyl compound caronaldehyde. This is also confirmed by literature data (Arey *et al*, 1990; Hakola *et al*., 1994; Calogirou *et al*., 1999). Formaldehyde and acetone have also been determined as reaction products (Reissel *et al*., 1999).

Product yields

The relative yields of formaldehyde, acetone and caronaldehyde at 50 and 100 Torr are given in Table III. Changes in the reaction time or in the initial concentration of H_2 (by up to a factor of 5) are found to have negligible effects on the yields. Caronaldehyde has been identified as an important oxidation product by other research groups, although with lower yields: $14 \pm 5\%$ (Larsen *et al*., 2001), $15 \pm 3\%$ (Orlando *et al*., 2000), 31% (Arey *et al*., 1990) and $34 \pm 8\%$ (Hakola *et al*., 1994).

Table III: Product yields for the Δ^3-carene/OH reaction products (mol %) at 50 and 100 Torr, $[\Delta^3\text{-}C_{10}H_{16}] \sim 2.2 \ 10^{12}$ molec/cm^3, $[H_2] = 1.37 \ 10^{13}$ molec/cm^3, $[NO_2] = 3.64 \ 10^{12}$ molec/cm^3, $[O_2] = 3.24 \ 10^{17}$ molec/cm^3 (50 Torr), $[O_2] = 6.48 \ 10^{17}$ molec/cm^3 (100 Torr), reaction time = 40 ms.

Reactor pressure (Torr)	50	100
Formaldehyde	13.0 ± 1.5	7.9 ± 1.6
Acetone	11.0 ± 1.8	7.1 ± 1.6
Caronaldehyde	75.9 ± 2.0	85.0 ± 2.8

The reported yields for formaldehyde ($12 \pm 3\%$ (Orlando *et al*., 2000) and $21 \pm 4\%$ (Arey *et al*., 1990)) and acetone ($15 \pm 3\%$ (Orlando *et al*., 2000)) are in better agreement with our results.

Influence of NO

The effect of NO between 3.6 10^{12} and 1.87 10^{13} molec/cm^3 was investigated at 50 Torr. The yield of caronaldehyde decreases with NO, while the formaldehyde and acetone yields increase. At the highest NO concentrations, formaldehyde and acetone become even more important than caronaldehyde. Besides the relative product yields, the absolute product amount collected was observed to slightly increase when NO is increasing.

Experiments were carried out using a lower concentration ratio of OH radicals. Introduction of lower NO_2 concentrations in the reactor (2.24 10^{12} molec/cm^3 instead of 3.64 10^{12} molec/cm^3) results in lower initial OH. The relative yield of caronaldehyde is found to be about 8.2% higher at low OH. This is probably due to a decreased impact of the caronaldehyde oxidation by OH in this case.

Proposed reaction mechanism

The reaction of Δ^3-carene with OH follows the classical pattern for alkenes: OH is added to the double bond, and the adduct reacts with molecular oxygen to form a peroxy radical. Upon reaction with NO, an alkoxy radical is formed, which can react in two ways. Either a methyl radical can be split off, leading to the formation of a ketone compound and formaldehyde, or a ring opening occurs followed by an H-atom abstraction by O_2, leading to caronaldehyde. Formation of acetone is more complex, but is expected to occur along the same lines as in the α-pinene/OH reaction system (Van den Bergh *et al.*, 2000; Vereecken and Peeters, 2000).

3.2.3 Limonene + OH

Identification of products

Endolim is seen to be the most important oxidation product of limonene, with the minor products formaldehyde, 4-AMCH and acetone. These products were also determined by other groups (Grosjean *et al.*, 1992; Spittler, 1997). In addition, a product of molecular mass M_r = 152 g/mol has been detected. Based on its fragmentation spectrum, its proposed structure is displayed in Figure 4.
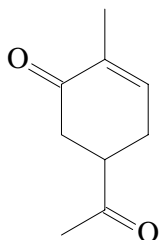
Figure 4: Proposed structure of the unknown limonene degradation product.

Several important difficulties arose in the analysis of the limonene-OH reaction products, in particular with regard to the ionization, stability, purity and separation of some of the compounds. In particular, it was seen that two important oxidation products of the limonene-OH reaction, 4-AMCH and endolim, were difficult to separate with HPLC. Since they show no complete baseline separation, quantitative determination using DAD detection is not possible.

Proposed reaction mechanism

A plausible reaction mechanism can be proposed for limonene, explaining the identified reaction products. Since limonene contains two double bonds, different OH-limonene adducts can be formed in the initial step. Addition to the double bond of the limonene ring ultimately leads to the formation of endolim, while addition to the double bond of the side group can lead to the formation of 4-AMCH and formaldehyde or acetone.

3.2.4 Kinetic modelling of α-pinene-OH reaction

The α-pinene/OH reaction system has been studied in a previous project (Van den Bergh *et al.*, 2000; Vanhees *et al.*, 2001). A kinetic modelling study has been carried out to check whether the product yields derived with the fast-flow reactor technique can be simulated. The α-pinene/OH mechanism from the MCM v3, consisting of 113 species and 164 reactions, has been implemented in the Facsimile 4.0 software program. Note that there are substantial differences between the MCM mechanism for α-pinene and the mechanism derived by the team of J. Peeters in the context of this project and described in Sect. 3.4 (e.g. the H-abstraction channels, the ring closure reactions, etc.). Furthermore, the pressure dependence of the mechanism (through e.g. the reactions of activated species and the nitrate-forming channel in the reactions of peroxy radicals with NOx) is not taken into account in the calculations,

although it might cause large differences between the yields at 760 and 50 Torr (as demonstrated by the observed pressure dependence of the product yields for the other terpenes between 50 and 100 Torr). Nonetheless, the kinetic calculations shown here can help to characterize the type of chemical behaviour and products formed in the fast-flow reactor.

The degradation of α-pinene has been simulated at 50 Torr and 298 K. The initial concentrations for OH, NO, NO$_2$, O$_2$ and α-pinene are in the range of the experiments. The figure below shows the time evolution of the relative yields of the main products for the conditions given in the figure caption.
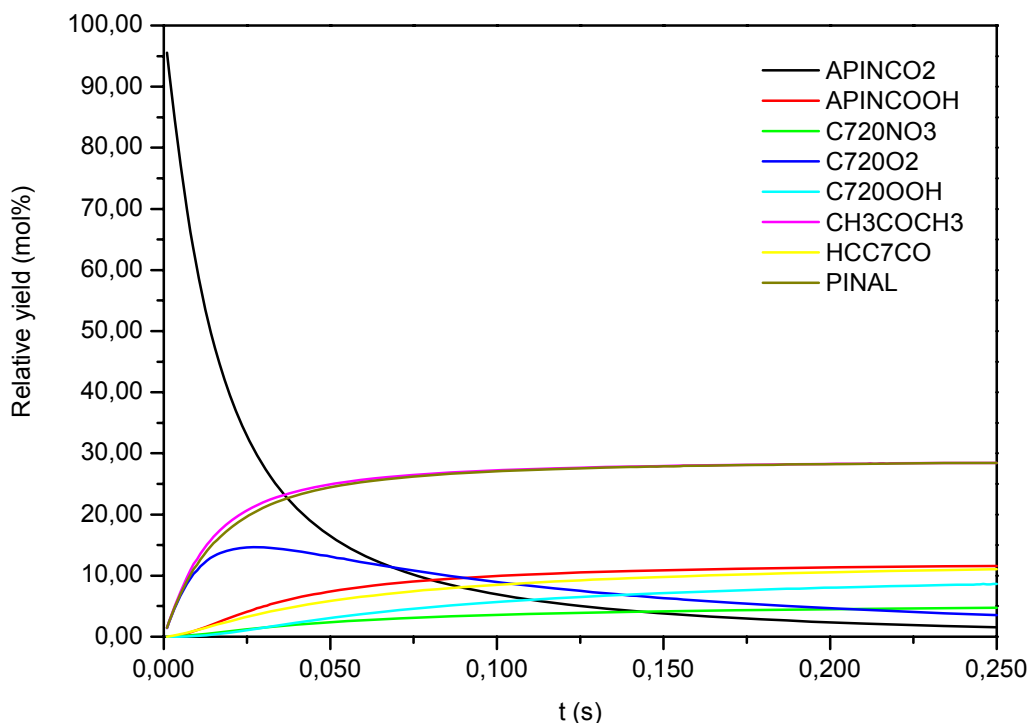
Figure 5: Relative product yields (mol %) as a function of time (s) as calculated from the simulation of the α-pinene-OH reaction, $[OH]_{in}$ = 3.62 10^{12} molec/cm^3, $[NO]_{in}$ = 3.62 10^{12} molec/cm^3, $[NO_2]$ = < 10^9 molec/cm^3, $[O_2]$ = 3.24 10^{17} molec/cm^3 and $[\alpha$-pinene] = 5.00 10^{12} molec/cm^3.

Eight main products are formed, with pinonaldehyde (PINAL) and acetone as the most important ones. APINCO2, which is a radical and cannot be detected with our analysis techniques, is initially dominant but decreases to a low level. Besides these

products, other compounds appeared in the simulation but with very low yields totalling only 2%. The formation of acetone and pinonaldehyde as most important reaction products is in agreement with the experiments, although pinonaldehyde was observed with a much higher yield than acetone (respectively 63±3% and 16±1%). The lower observed acetone yield is a likely consequence of a ring closure reaction not included in the MCM, which inhibits acetone formation in relatively low NOx situations, as shown by J. Peeters' group. Formaldehyde, acetaldehyde and campholene aldehyde have been identified in our experiments but are found to be negligible in the simulation. Acetaldehyde was experimentally determined in Sect. with only a very small yield (~1%). Formaldehyde was seen to be the third most important reaction product with a yield of around 10%, in contrast with the simulation.

Six (out of 8) simulated compounds could not be determined by our analysis technique, including a carbonyl, two hydroxy hydroperoxides, a hydroxy nitrate, and two peroxy radicals. The carbonyl is actually not formed in the mechanism described in Sect. 3.4. The simulated product distribution would certainly be very different had the mechanism by J. Peeters' group been used instead of the MCM, but it can be assumed that on the order of 50% (molar) of the simulated products could not detected, mainly consisting of hydroxy hydroperoxides and hydroxy nitrates. This would bring the experimental pinonaldehyde yield in tune with the simulated value, but the experimental acetone yield is much too low.

3.3 LABORATORY STUDY OF MONOTERPENE-OH REACTIONS (E.A., BRUSSELS)

3.3.1 Study of ion/molecule reactions in support of the CIMS detection of VOCs and their oxidation products

3.3.1.1 Rate constants

Rate constant measurements have been performed for the reactions of H_3O^+, NO^+ and O_2^+ ions with a series of monoterpenes, monoterpene oxidation products, atmospherically relevant aldehydes and with oxygenated BVOCs or oxVOCs (29 species in total). In addition the rate constants of $H_3O^+.H_2O$ and $NO^+.H_2O$ ions with some aldehydes and with oxVOCs have been determined.

The accuracy of the reaction rate constant measurements is estimated to be 20% (25% for the monoterpene oxidation products nopinone, 4-acetyl-1-methyl-cyclohexene, α-pinene oxide, PIN and CAR).

In ion/molecule reaction studies it is customary to compare the experimental reaction rate constant k_{exp} with the collision reaction rate constant k_C (Su and Chesnavich, 1982, Su, 1988). The value of k_C depends on the polarizability and dipole moment of the neutral reactant. Since literature data of these parameters for the reactants studied are very sparse, they have been derived from quantum chemical calculations taking into account possible rotameric forms or geometric isomerism of the neutral reactants. All ion/molecule reactions studied, except the NO^+/glyoxal reaction, are found to proceed at a rate close to collision rate.

3.3.1.2 Product distributions

Monoterpenes

The major channel in the reaction of H_3O^+ with the monoterpenes is non-dissociative proton transfer. $C_6H_9^+$ fragment ions are observed to a lesser degree. The NO^+ reactions are mainly characterized by non-dissociative charge transfer. The reactions with O_2^+ proceed via dissociative charge transfer giving rise to several ionic products, which are also observed in the electron impact spectra of these monoterpenes.

Oxidation products of monoterpenes

H_3O^+ reacts with 4-acetyl-1-methyl cyclohexene and nopinone by non-dissociative proton transfer. The major channel in the reaction of H_3O^+ with α-pinene oxide, PIN and CAR is elimination of a water molecule following protonation. The reaction of NO^+ with 4-acetyl-1-methyl cyclohexene and nopinone is mainly determined by non-dissociative charge transfer. Non-dissociative charge transfer is also observed in the reaction of NO^+ with α-pinene oxide, PIN and CAR, as well as a series of fragment ions. A non-negligible hydride ion transfer channel occurs in the spectra of NO^+ with PIN. Three-body association is also observed in the reactions NO^+/nopinone and NO^+/CAR. The $O_2^{\bullet+}$ spectra show multiple products, mainly characterized by charge transfer and extensive fragmentation.

Methyl Vinyl Ketone (MVK) and the aldehydes Methacrolein (MaCR), pivaldehyde, 2-methyl butanal, glyoxal, o-, m- and p-tolualdehyde

All H_3O^+ reactions with these reactants proceed by proton transfer, non-dissociative for all compounds, except for 2-methyl-butanal, where two minor channels are observed due to fragmentation after protonation. Three-body association is the only pathway in the NO^+/MVK and NO^+/glyoxal reactions. Hydride ion transfer is the dominant process occurring in all the other NO^+ reactions. Elimination of CHO for pivaldehyde and association for MaCR are also non-negligible channels in their reaction with NO^+. All O_2^+ reactions result in the parent cation and in at least one fragment ion. Possible hydratation of the product ions, when water is introduced in the reaction zone, has also been studied.

Oxygenated BVOCs: 2-methyl-3-buten-2-ol, cis-3-hexenol, cis-3-hexenyl acetate, 1,8-cineole, 6-methyl-5-hepten-2-one, camphor, linalool, nerol and geraniol

Only the H_3O^+/camphor reaction results exclusively in the protonated parent cation. The main reaction mechanism for all other H_3O^+/oxVOC reactions is H_2O elimination following proton transfer. The NO^+/2-methyl-3-buten-2-ol reaction solely proceeds through hydroxide transfer. Except for cis-3-hexenyl acetate and linalool, the dominant process for all other NO^+ reactions is charge transfer. Some other mechanisms have also been observed for the NO^+/oxVOC reactions, e.g. elimination of a H_2O molecule following charge transfer, three-body association, hydride transfer, CH_3 elimination. The O_2^+/oxVOC reactions all resulted in extensive fragmentation of the nascent excited parent cation.

These product ion distributions allow us to determine:
- which precursor ion (H_3O^+, NO^+ or O_2^+) and corresponding product ion(s) are most suited to detect and quantify a given reactant by the CIMS technique
- if these precursor ions can be used to distinguish between isomers in laboratory and/or field measurements.

3.3.2 Acetone + OH

The acetone + OH reaction has been studied at 8.1 Torr in the FFR/CIMS instrument. NO_2 and acetone are introduced through the central injector in order to avoid loss of OH at the reactor walls. Acetone is present in large excess (4×10^{15}-

2×10^{16} molecules cm^{-3}) with respect to NO_2 (9.1×10^{11} molecules cm^{-3}) to avoid OH loss by reaction with NO and NO_2. In these conditions $\Delta[acetone] = \Delta[NO_2] = \Delta[OH]$. The reaction time is estimated to be 40 ms. The OH production in the absence of acetone is controlled through monitoring of the OH^- and NO_2^- ion signals (charge transfer products of SF_6^- with OH and NO_2 respectively). The H atom production is adjusted in such a way as to have complete NO_2 conversion, i.e. $\Delta[NO_2] = [NO_2]_i$. The acetic acid yield is defined as:

$$Y = \frac{\left[CH_3C(O)OH\right]_{CIMS}}{\left[NO_2\right]_{i,CIMS}}$$

$[CH_3C(O)OH]_{CIMS}$ is obtained using CF_3O^- and SF_6^-, which both react with $CH_3C(O)OH$ through fluoride transfer, resulting in $CH_3C(O)OHF^-$ (m = 79 u).

An average acetic acid yield of 1 ± 0.5 % is found. It is an upper limit, since the mass peak at 79 u may be a superposition of the signal of $CH_3C(O)OHF^-$ and of other ions having the same molecular mass. Mass discrimination and diffusion enhancement effects are unknown in these experiments and are therefore not considered in the analysis. When using CF_3O^- (m = 85 u) the difference in molecular mass between source and product ions is small and therefore these effects are not expected to have an important impact on the yields.

It can be concluded that, at room temperature, the proposed addition-elimination pathway of the OH + acetone reaction (which should result in acetic acid and CH_3 radicals) is characterized by a very low yield.

3.3.3 α-pinene + OH

The reaction of α-pinene with OH has been studied at FFR pressures of 2 and 50 Torr in the presence of oxygen, with and without additional NO. The experimental conditions are summarized in Table IV. Acetone, formaldehyde and pinonaldehyde are detected with CIMS (using H_3O^+ precursor ions) at mass 59 ($H^+.CH_3C(O)CH_3$), 31 ($H^+.HC(O)H$) and 151 (dehydrated protonated pinonaldehyde) respectively. The product yields are given in Table V, and compared with the results of Vinckier and co-workers in a similar FFR set-up, by EI-MS (at 2 Torr) and by collection and derivatization of the reaction products on a cold trap followed by detection by HPLC-MS (50 Torr).

At 2 Torr no explicit reaction time dependence of the yields is noticed. The acetone and formaldehyde yields are found to be independent of the initial $[H_2]$ concentration (and thus of the initial hydroxyl concentration). The pinonaldehyde yield, however, monotonically decreases from 25 % at low $[H_2]$ to 16 % at high $[H_2]$.

In the 50 Torr case, no explicit dependence of the yields on the reaction time and on the initial OH concentration is noticed. In the presence of additional NO (referred to as the high [NO] condition), the acetone and formaldehyde yields slightly increase with extra NO, while the pinonaldehyde yield decreases. This is in agreement with what has been obtained previously by the group of Vinckier and co-workers using an identical reactor but a totally different off-line detection technique.

Table IV: Experimental conditions. Concentrations are expressed in molecules cm^{-3}.

Pressure (Torr)	50	2
$[O_2]$	3.2×10^{17}	4.0×10^{15}
$[NO_2]_{ini}$	3.2×10^{12}	8.0×10^{12} - 1.2×10^{13}
$[H_2]_{ini}$	1.1×10^{12} - 8.7×10^{13}	2.0×10^{12} - 3.2×10^{13}
$[\alpha\text{-pinene}]_{ini}$	$\approx 3 \times 10^{12}$	3.0×10^{12} - 7.1×10^{12}
Reaction time (ms)	24 – 49	5.5 - 14.5
$[NO]_{extra}$	1.1×10^{13}	

Table V: Experimentally determined yields (in %); [a] [Vinckier *et al.*, 1998]; [b] [Vanhees *et al.*, 2001]; [c] [Peeters *et al.*, 2001]. The pinonaldehyde yields between braces are obtained by using the calculated collision rate constant of the H_3O^+/pinonaldehyde reaction instead of the experimentally derived rate constant (which is a lower limit).

compound	This work, team of E. Arijs			Vinckier group (KULeuven)			Lit. values[c]
	2 Torr	50 Torr		2 Torr[a]	50 Torr[b]		
		Low [NO]	high [NO]		low [NO]	high [NO]	
acetone	28 ± 3	14 ± 2	17 ± 2	18 ± 2	16 ± 1	20.8	[5-17.9]
formaldehyde	17 ± 4	6.7 ±1.4	9.4 ± 1.7		9.7 ± 0.7	14.4	[6-23]
pinonaldehyde	22 ± 5 {16 ± 3}	24 ± 2 {17 ± 2}	20 ± 3 {14 ± 2}	31 ± 15	63 ± 3	55.7	[6-87]

The errors in this table are due to statistical variation. However, due to the rather large errors on the ion/molecule rate constants and on the product ion distributions, the total error on the yields can be as high as 50%. For acetone, however, this global error can be reduced to 20% because quantification of acetone and α-pinene with the CIMS-method has been found to be quite accurate, as demonstrated by

introducing well-known amounts of these species into the CIMS reactor. As with any CIMS-based quantification, the 'fingerprint' ion peaks can be superpositions of several isomeric ion species peaks, and therefore the yields given above have to be considered as upper limits.

3.3.4 β-pinene + OH

The reaction of β-pinene with OH has been studied at 200 Torr with the HPTFR/CIMS instrument. It is well-suited for studying kinetics of OH/VOC reactions at high pressures, as verified by our measured rate constant for OH + β-pinene, 8.4×10^{-11} cm^3 $molecule^{-1}$ s^{-1}, in very good agreement with previously reported values (e.g. 7.95×10^{-11} (Atkinson *et al.*, 1986), 8.3×10^{-11} (Grosjean and Williams, 1992)).

The yields of nopinone and acetone have been measured at several reaction times (20-60 ms), initial β-pinene concentrations (8×10^{11}-5×10^{12} molecules cm^{-3}) and OH concentrations, and with additional NO (1-6×10^{13} molecules cm^{-3}) and without additional NO. Moreover, both H_3O^+ and NO^+ were used as precursor ion species, hereby excluding erroneous quantification of oxidation products due to ion chemistry complications.

Table VI: Experimentally determined yields (in %). The error on the data corresponds to the standard deviation and can be considered here as the total accuracy of the yields. The yields have to be considered as upper limits.

compound	Low [NO]	High [NO]	Lit. values
Acetone	15.4 ±1.2	16.2 ± 2.0	[2-13]
Nopinone	6.3 ± 2.5	10.4 ± 2.7	[17-79]

Because of experimental difficulties associated with the introduction of CH_2O, the instrument could not be calibrated for this compound. However, from the variation of the $H^+.HC(O)H$ ion signal in different conditions, it is concluded that the yield of CH_2O at high [NO] is about 3 times higher than at low [NO]. By comparing the ion signals of $H^+.HC(O)H$ and $H^+.CH_3C(O)CH_3$, the formaldehyde yield at high [NO] is expected to be close to the acetone yield.

3.4 THEORETICAL STUDY OF THE OH-INITIATED OXIDATION OF MONOTERPENES AND CONSTRUCTION OF EXPLICIT MECHANISMS

3.4.1 Development of a generalized SAR for the decomposition of substituted alkoxy radicals

A novel and readily applicable quantitative Structure-Activity Relationship (SAR) for predicting the barrier height E_b to decomposition by β C-C scission of substituted alkoxy radicals was developed as a prime tool for the objective construction of explicit mechanisms of the atmospheric oxidation of large (biogenic) VOC. The SAR is based on computed energy barriers, using a proven level of theory for this type of process (see *sub* 2.4.2), and was validated against barriers derived from experimental data. The SAR is expressed solely in terms of the number(s) N_i of alkyl-, hydroxy- and/or oxo-substituents on the α- and β-carbons of the breaking bond: $E_b(kcal/mol) = 17.5 - 2.1 \times N_\alpha(alk) - 3.1 \times N_\beta(alk) - 8.0 \times N_{\alpha,\beta}(OH) - 8.0 \times N_\beta(O=) - 12 \times N_\alpha(O=)$. For barriers below 7 kcal/mol, an additional, second-order term accounts for the curvature. The SAR reproduces the available experimental and theoretical data within 0.5 to 1 kcal/mol. The SAR generally allows conclusive predictions as to the fate of larger alkoxy radicals (see *sub* 2.4.1). The dissociation rate at absolute temperatures T around 300 K is found from the predicted E_b using $k_{diss}^{\infty}(T) = 1.8 \times 10^{13} \exp(-E_b/RT)$ s^{-1}.

For radicals subject to ring-strain or specific radical stabilization effects, the SAR may fail; therefore, for such cases, quantum-chemically computed E_b were used in the following subsections.

3.4.2 Construction of Objective Detailed Mechanism for the OH-Initiated Oxidation of α-Pinene

An explicit mechanism was developed for the OH-initiated atmospheric oxidation of α-pinene in the presence of NO$_x$, based solely on objective chemical knowledge, on the quantitative SARs *sub* 2.4.1, or on the first-principle methods outlined *sub* 2.4.2. The fate of some 40 organic radical intermediates needed to be quantified. The primary reaction yields mainly two chemically activated αpinene-OH adduct radicals (~45% each), of which one partly undergoes prompt 4-ring opening and finally forms acetone (Vereecken and Peeters, 2000). Overall, the initial adduct radicals lead mainly to pinonaldehyde, acetone, formaldehyde, formic acid, and nitrates. Primary-

step H-abstraction by OH is found to be minor (~10%) but to produce much of the formaldehyde. Total first-generation product yields were obtained by propagating the product fractions of each step in the mechanism.

Table VI lists the overall product yields predicted for the high-NO levels ($\approx$1 ppm) of usual laboratory experiments and for the lower NO levels (0.2 - 2 ppb) in real (polluted) atmospheres. The substantial differences are mainly due to the different fates of the α-hydroxyalkylperoxy radicals from the thermalized initial adducts: fast reaction with NO at high levels (Capouet *et al.*, 2004) versus decomposition (see also 3.6.2) at low NO. Table VII shows that our predictions compare favourably with the averages of the available laboratory measurements.

Table VI. Molar product yields in the reaction between α-pinene and OH radicals predicted in this study, for (high-NO) laboratory and (moderate-NO) real atmospheric conditions.

	Theoretically Predicted Yields (%)	
	Laboratory	Atmosphere
Pinonaldehyde	35.7	59.5
Acetone	17.9	11.9
CH_2O	18.8	12.6
Organic nitrates	19	13.1
HCA168	11.3	11.3
CO_2	30.7	8.7
HC(O)OH	9.2	-
$CH_3C(O)OH$	8	-
other carbonyls[a]	25.9	16.4

[a] unsaturated dicarbonyls, unsaturated (poly)hydroxycarbonyls (cyclic and non-cyclic), methyl vinyl ketone, methacrolein, glycolaldehyde, malonaldehyde

Table VII. Summary of available laboratory measurements of molar product yields in the reaction between α-pinene and OH radicals at high NO_x levels

	Product Yield (%)			
	Pinonaldehyde	Acetone	CH_2O	HCOOH
Arey et al.	29 ± 5	-	-	
Hatakeyama et al.	78.5^a	-	-	
Hakola et al.	28 ± 5	-	-	
Vanhees et al. (100 Torr)	82 ± 7	6 ± 2	6 ± 5	
Aschmann et al.	-	11 ± 2.7	-	
Fantechi, 1999	-	5	-	6
Nozière et al.	87 ± 20	9 ± 6	23 ± 9	
Orlando et al.	-	5 ± 2	19 ± 5	7 ± 2
Larsen et al.	6 ± 2^c	11 ± 3	8 ± 1	28 ± 3^c
Wisthaler et al.	34 ± 9	11 ± 2	-	
This work (lab. conditions)	**35.7**	**17.9**	**18.8**	**9.2**

[a] see also Nozière et al. (1999); [b] Unpublished results; [c] due to strong oxidative conditions

3.4.3 Mechanism of OH-initiated Oxidation of Pinonaldehyde

The oxidation mechanism of OH + pinonaldehyde, which is the major product of α-pinene + OH, was constructed using the same methods as above. The primary OH-attack abstracts H-atoms from six different carbon atoms. For each of these H-abstraction sites, a detailed mechanism of product formation in atmospheric conditions was developed. Invoking only 'classical' alkyl-, alkylperoxy- and alkoxy chemistries, the objective fate of some 30 organic radical intermediates was predicted. Total primary product yields were obtained by propagating the products fractions of each step in the mechanism. Overall predicted product molar yields for high-NO (laboratory) conditions are: 23% 4-hydroxynorpinonaldehyde, 10% acetone, 13% CH_2O, 30 % organic nitrates, 74% CO_2, 11% HC(O)OH, 17% norpinonaldehyde and CO, and 17% other (hydroxy)(poly)carbonyls. Here also, our results are in good accord with the experimental data, with the exception of CH_2O, for which Nozière et al. (1999) reported a ten times higher yield — that remains so far unconfirmed. In more realistic atmospheric conditions, at lower NO levels, our theoretically predicted yields differ only regarding 4-hydroxynorpinonaldehyde (38%), HC(O)OH (<1%), and nitrates (26%).

3.4.4 Novel Ring-closure Reactions of Peroxy and Oxy Radicals in the Oxidations of Isoprene and β-Pinene

Peroxy and oxy radicals play a crucial role In the atmospheric oxidation of organic compounds. The traditional views are that peroxy radicals react with NO or with other (hydro-)peroxy radicals, while oxy radicals decompose, undergo a hydrogen shift, or react with O_2. However, in a thorough quantum chemical and statistical-rate investigation, we discovered that unsatured (per)oxy radicals formed from isoprene and monoterpenes can undergo hitherto unsuspected ring closure reactions. These processes are shown to be competitive in atmospheric conditions, and to have a substantial or even major impact on the oxidation products. We thus found that isoprene oxidation at low NO_x can proceed for some 5-10% through hitherto unknown peroxy ring-closure mechanisms. Furthermore, we showed that the OH-initiated oxidation of β-pinene should proceed dominantly through newly revealed oxy ring-closure pathways, thus offering a consistent rationalization for the 'anomalously' low observed yields of traditional-route oxidation products from this compound.

3.5   SIMULATION OF ALPHA-PINENE OXIDATION EXPERIMENTS

3.5.1 α-pinene + OH

The extensive set of photooxidation experiments performed by Nozière *et al.* (1999) has been used to test both the mechanism and the model described in Sect. 2.4 and 2.5. It is well suited for this purpose, since it consists in a total of 37 experiments conducted at standard pressure and temperature conditions, in presence and in absence of NO. These experiments used either H_2O_2 and UV light, or CH_3ONO and visible light as radical precursor.

The comparison of the calculated vs. measured concentrations as a function of time shows that the levels of OH, NO, NO2 and light are well reproduced by the model. As an illustration, Figure 6 displays the evolution of the measured and calculated concentrations of several important compounds for two specific experiments.
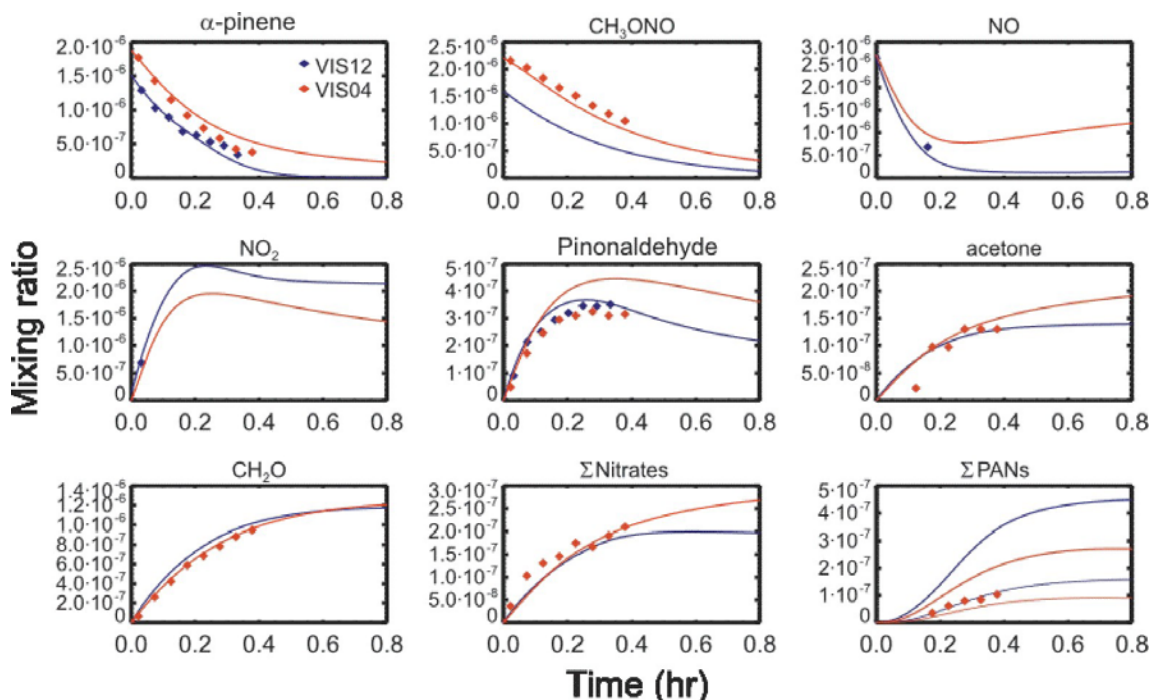

Figure 6: Measured (diamonds) vs. simulated concentrations as a function of time for two α-pinene oxidation experiments in presence of NO with visible light.

In spite of the large scatter in the experimental results and the difficulty to retrieve true product yields from concentration data, we show that the model succeeds in

reproducing the average apparent yields of pinonaldehyde, acetone, total nitrate and total PANs in the experiments performed in presence of NO, comforting our confidence in the proposed mechanism in such conditions. In absence of NO, pinonaldehyde is fairly well reproduced, but acetone is largely underestimated. This is a likely consequence of the non-explicit treatment of the chemistry following specific reactions in the mechanism (ring closure, oxidation of primary products).

3.5.2 α-pinene + O$_3$

The ozonolysis experiments of Yu *et al.* (1999) include both gas-phase and particulate product yield measurements, and are therefore appropriate for testing the gas-particle partitioning module (Sect. 2.5.2). As seen on the figure below, the total aerosol concentration is slightly underestimated by the model. Carboxylic acid dimers are predicted to be dominant in the aerosol phase in these experiments.
However, the model fails to reproduce the high aerosol yields observed by Hoffman *et al.* (1999), for reasons unknown but possibly related to the high reactor temperatures (320 K) used in these experiments. Further work will be necessary to improve the aerosol model and account for the effects of (i) dissolution of oxidation products in the liquid phase of the aerosol and (ii) particle-phase reactions leading to the formation of less volatile compounds like oligomers and polymers.
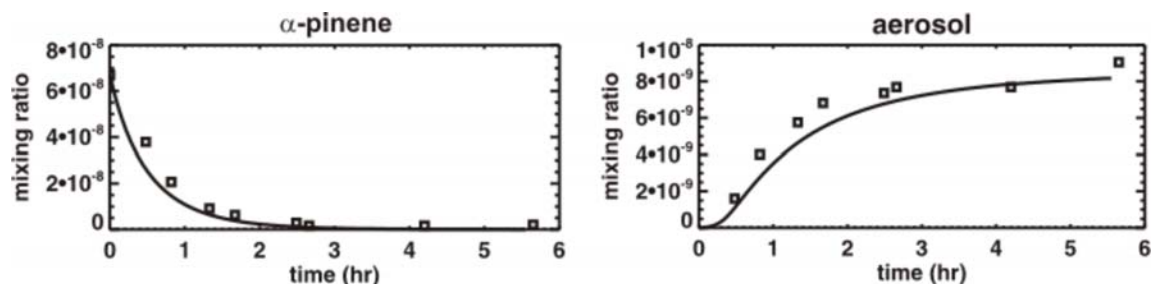

Figure 7: Modelled (curves) and measured (squares) mixing ratios of α-pinene (left) and total aerosol (right) in experiment B from Yu *et al.* (1999).

3.6   STUDY OF OH and HO$_2$ REACTIONS OF IMPORTANT OXYGENATED ORGANICS IN THE UT/LS

3.6.1 Reactions of OH radicals with acetaldehyde, propionaldehyde, acetone and acetic acid

Aldehydes

The branching fraction of H-abstraction in the elementary reactions of acetaldehyde and propionaldehyde with OH at 290 K was measured directly by quantifying the primary-product H$_2$O yields of these reactions using DF–MBMS. The yields were found to be 89 ± 6 % and 100 ± 10 % for the reactions of acetaldehyde + OH and propionaldehyde + OH, respectively. Furthermore, an upper limit of 3 % was found for the yield of formic acid that would result from the addition/elimination mechanism put forward by Taylor et al 1996 as dominant pathway. We conclude therefore that, contrary to Taylor et al, these reactions proceed quasi-exclusively by H-abstraction to form acyl radicals R-CO, the known precursors of PANs.

Acetone

In the experimental investigation of the controversial reaction of acetone with OH at 290 K, no significant production of acetic acid could be measured; by absolute calibrations we found an upper limit for the branching fraction of the OH-addition/CH$_3$-elimination channel of <5%. This direct result refutes the high acetic acid yields recently suggested by Wollenhaupt and Crowley (2000) and by Vasvary et al. (2001). In a complementary theoretical study, the potential energy profiles of the OH-addition/CH$_3$-elimination channel, the direct H-abstraction channel, and the indirect H-abstraction path *via* an hydrogen-bonded OH-acetone complex, were characterized at appropriate levels of QC theory. The barrier for OH-addition on the C=O double bond is found to be at least 2.5 kcal/mol higher than that for the H-abstraction channels. Subsequent TST theory and RRKM-master equation calculations show that the OH-addition channel is negligible at all relevant atmospheric temperatures. The OH + acetone reaction is shown to proceed through a pre-reactive H-bonded complex, followed by H-abstraction of a methyl hydrogen. The rate is strongly influenced by the H-bonding and by tunnelling through the energy barriers, which rationalizes the negative temperature dependence of the rate coefficient observed by Wollenhaupt et al. (2000) at temperatures below 250K.
Flow reactor – CIMS studies performed at the Belgian Institute for Space Aeronomy (team of E. Arijs) in this project confirm the absence of acetic acid as reaction

product (see Sect. 3.3.2). Some five other groups have since then concurred with our findings on this controversial issue.

Acetic Acid

The product distribution of the reaction of acetic acid, CH_3COOH, with hydroxyl radicals, OH, was also studied experimentally and theoretically. DF – MBMS measurements at 290 K of the CO_2 yield versus loss of acetic acid resulted in a branching fraction of (64 ± 14) % for abstraction of the acidic hydrogen: $CH_3COOH+OH \rightarrow CH_3COO + H_2O \rightarrow CH_3+CO_2+H_2O$. A quantum chemical and theoretical kinetic analysis showed that abstraction of the acidic hydrogen is enhanced relative to abstraction of a methyl-H due to the formation of a strong pre-reactive H-bonded complex. Addition of OH-radicals on the C=O double bond is shown to be negligible at ambient temperatures. Thus, this reaction is shown to lead directly to CH_3 formation for a major fraction. Our generalized oxy-decomposition SAR predicts that the OCH2COOH radicals resulting from the competing abstraction of a methyl-H should exclusively yield CH_2O, CO_2 and HO_2 in all atmospheric conditions, such that (the readily photolyzable) glyoxylic acid can not be formed.

We thus conclude that for molecules bearing carbonyl- and carboxyl functionalities, addition/elimination reactions of OH-radicals on the C=O double bond are far outrun by H-abstractions, such that OH reacts with aldehydes, ketones and acids quasi-exclusively by H-abstraction. The rate coefficient k(T) and its temperature dependence is strongly influenced by formation of pre-reactive H-bonded complexes and tunnelling through the potential energy barrier from these complexes. This leads to an unexpected *increase* of k(T) at the lower temperatures of the UT/LS, especially pronounced for the cases of acetone and acetic acid. For the latter, we are presently confirming the strong negative temperature-dependence in further experiments.

3.6.2 Effective HO_2-initiated removal of acetone and formaldehyde near the tropopause

Whereas the reactions of hydroperoxyl radicals with formaldehyde (Veyret et al. 1989) and acetaldehyde (Tomas et al., 2001) are known to occur, reactions of HO_2 with ketones on the other hand are generally believed to be negligibly slow in all conditions (Gierczak and Ravishankara, 2000).
We have computed detailed PES for the addition of HO_2 radicals to CH_2O, CH_3CHO, $(CH_3)_2CO$ and c-hexanone, using several high-level *ab initio* methods (G3, CBS-QB3 and a near-converged G2M variant). The reactions were all found to proceed through

a cyclic H-bonded complex, which, via a rate-controlling TS_a, gives an α-hydroxy-alkylperoxy radical, $Q(OH)OO$ (where Q stands for R_{-H}), in various rotameric forms. Table VIII shows the data for acetone:

$$(CH_3)_2CO + HO_2^\bullet \rightleftharpoons (CH_3)_2C(OH)OO^\bullet \qquad \text{(r 3.6.2.1)}$$
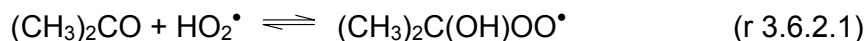
the three levels of theory agreeing to within 0.1 – 0.4 kcal/mol.

Rate constants for forward and reverse reactions and the equilibrium constant were obtained by multi-conformer TST theory. The results agree within 30% with the available experimental data (for CH_2O and CH_3CHO; see above). Both the forward and reverse reactions are fast, resulting in rapid (pre-)equilibria. For the ketones, redissociation at 300 K is predicted to be so fast that no reaction should be apparent, in accord with experimental results (Gierczak, 2000). At ambient temperatures, the equilibrium [Q(OH)OO] concentrations are negligible, but below ≈220 K, as in the tropopause, they become high enough for the subsequent fast reactions

$$Q(OH)OO + NO \rightarrow Q(OH)O + NO_2 \qquad \text{(r3.6.2.2)}$$
$$Q(OH)OO + HO_2 \rightarrow Q(OH)OOH + O_2 \qquad \text{(r3.6.2.3)}$$
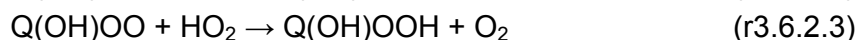
to constitute efficient indirect sinks for the carbonyl, thereby also producing an organic acid by the fast β C-C dissociation of the Q(OH)O radicals (formic acid from CH_2O, acetic acid from acetone) or, alternatively, depleting the HO_x radical pool (r 3.6.2.3).

Table VIII ZPE-corrected relative energies (kcal/mol) of the stationary points for the acetone + $HO_2^\bullet \rightleftharpoons (CH_3)_2C(OH)OO^\bullet$ reaction (in reverse order) at different levels of theory.

Structure	G3	CBS-QB3	G2Mc//DFT (extrap.)
$(CH_3)_2C(OH)OO^\bullet\_pm$[a]	0.0	0.0	0.0
$(CH_3)_2C(OH)OO^\bullet\_pt$	1.7[b]	idem	idem
$(CH_3)_2C(OH)OO^\bullet\_pp$	2.2[b]	idem	idem
TSa	11.4	11.5	11.15
c-$((CH_3)_2C=O$---$HOO^\bullet)$	4.1	4.5	4.3
$(H_3C)_2C=O + HOO^\bullet$	14.0	14.0	14.1

[a] The various rotational conformers all have mirror images, included in the TST calculations
[b] The E_{rel} of the $CH_3CH(OH)OO^\bullet$ conformers with respect to the lowest-lying are computed at the B3LYP/cc-pVTZ level.

It was found that this new, HO_2-initiated oxidation mechanism can indeed be important for formaldehyde, acetone, and c-hexanone (a template for nopinone from β-pinene), at temperatures of 210 K and lower. For these cases, the removal rate by

this mechanism in the wintertime tropopause above the temperate, polluted continental areas, at an adopted temperature of 210 K, is predicted to be about equal to that of the OH-reaction, and approaching the photolysis rate, while even overtaking both the latter at 200 K. Modelling using the IMAGES global model (J-F. Müller of BISA) confirms the importance of this reaction type also in the summertime tropical tropopause, where it is found to account for ≈30% of the acetone removal (see Fig. 8) and CH_2O removal, to be a minor source of acetic/formic acid, and to affect the HO_x budget significantly.
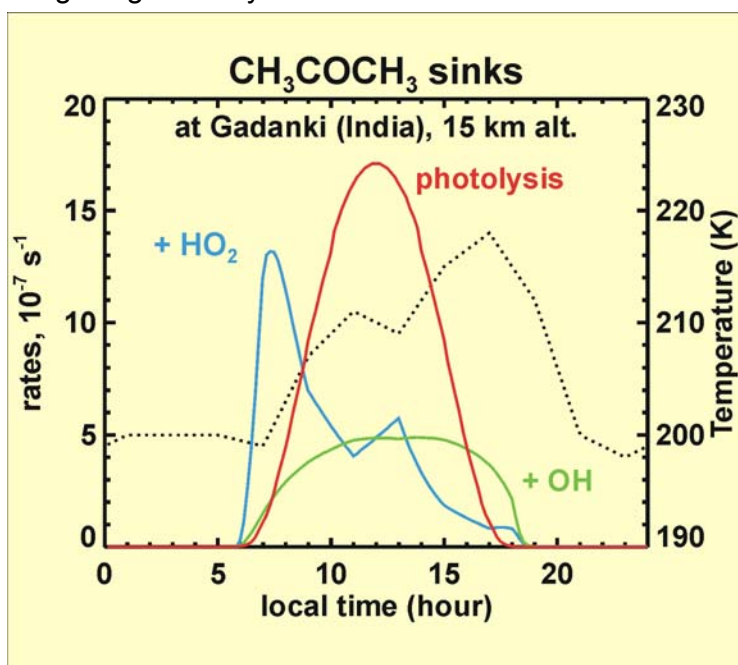

Figure 8: Modelled diurnal evolution of the removal rates of acetone for summer conditions near the tropopause above Gadanki, India. Photolysis dominates, except during early morning, where HO_2-initiated removal is predicted to be faster. Reaction with OH is the least important acetone sink, except during the afternoon and evening. The dotted line is the measured temperature, right-hand scale.

Our predictions cannot claim an accuracy better than a factor of 3; at 210 K this corresponds to 0.5 kcal/mol error in the relative energies of the Q(OH)OO with respect to HO_2 + carbonyl). Experimental verification must be awaited.

3.6.3 Organic hydroperoxide compounds

Reactions of hydroperoxide compounds with OH are known to proceed for a major part by H-abstraction from the α-carbon. The fate of the resulting radicals, however, is poorly understood, except for CH_2OOH. We performed a theoretical DFT and

Coupled Cluster theory analysis of the stability of the (resulting) radicals with hydroperoxyl- (HOO-) or alkylperoxyl (ROO-) substituents on the radical carbon, which revealed that all such radicals are unstable, dissociating spontaneously by O–O scission to a carbonyl compound and a hydroxy or alkoxy radical, even for multiple substituted compounds. Therefore, it can be concluded that the atmospheric reactions of (hydro)peroxides with OH are sources of carbonyl compounds.

4. CONCLUSIONS

This project has contributed to significant improvements in our understanding of the processes controlling the budget of tropospheric oxidants (O_3 and OH) and the formation of organic aerosols. The primary foci of this project are 1/ the emissions, chemistry and aerosol formation potential of biogenic volatile organic compounds (BVOC) and 2/ the impact of volatile organic compounds in the upper troposphere.

A first important achievement of this project is the development of innovative tools aiming to verify and improve the BVOC emissions estimates, either by confrontation with direct flux measurements or by inverse modelling in a global model using atmospheric observations of the BVOC oxidation by-products (CH_2O and CO). A second achievement of this project is the experimental detection and quantification of products in the oxidation of several monoterpenes (α- and β-pinene, Δ^3-carene and limonene) by OH, using newly developed analysis procedures. A third achievement is the construction of semi-explicit degradation mechanisms for several monoterpenes by advanced theoretical methods, and their verification by detailed simulations of laboratory experiments in a chemical box model. In the development of these mechanisms, novel chemical pathways have been discovered, which were unsuspected until now in spite of their high relevance in atmospheric conditions. A fourth achievement is the realization of a gas-aerosol partitioning model for the monoterpene oxidation products, of comparable or even better performance than previously used models. A fifth achievement is the determination of specific reactions of carbonyls relevant in the upper troposphere – in particular the reactions of acetone with OH and the reactions of several carbonyls with HO_2, reactions overlooked so far which we demonstrated as being potentially important. A final achievement in this project is the model prediction of the future possible evolution of the tropospheric composition in response to changing anthropogenic emissions, in the framework of international assessments (IPCC[2], ACCENT[3]).

---

[2] http://www.ipcc.ch/
[3] http://www.accent-network.org/

5. PUBLICATIONS IN THE CONTEXT OF THE PROJECT

Emission modelling:

Pétron G., Granier C., Khattatov B., Lamarque J.-F., Yudin V., Müller J.-F., Gille J., Inverse modeling of carbon monoxide surface emissions using CMDL network observations, *J. Geophys. Res.*, 107, D24, 4761, doi:10.1029/2001JD001305, 2002.

Müller J.-F., Stavrakou T., Inversion of CO and NOx emissions using the adjoint of the IMAGES model, *Atmos. Chem. Phys.*, 5, 1157-1186, 2005.

Wallens, S., Modélisation des émissions de composes organiques volatils par la végétation, PhD Thesis, Université Libre de Bruxelles, Sep. 2004.

Laboratory studies of monoterpenes-OH reactions:

Vanhees I., Van den Bergh V., Schildermans R., De Boer R., Compernolle F. and Vinckier C., Determination of the oxidation products of the reaction between α-pinene and OH radicals by High Performance Liquid Chromatography, *J. Chromat. A*, 915, 75-83, 2001.

Van den Bergh V., Coeckelberghs H., Vanhees I., DeBoer R., Compernolle F., Vinckier C., HPLC-MS determination of the oxidation products of the reaction between α- and β-pinene and OH, *Anal. Bioanal. Chem.*, 372, 630-638, 2002.

Van den Bergh V., Coeckelberghs H., Vankerckhoven H., Compernolle F., Vinckier C., Study of the carbonyl products of terpene/OH radical reactions: detection of the 2,4-DNPH derivatives by HPLC-MS, *Anal. Bioanal. Chem.*, 379, 484-494, 2004.

Laboratory studies of ion/molecule reactions in support of CIMS detection of organic compounds:

Schoon N., Amelynck C., Vereecken L., Arijs E., A selected ion flow tube study of the reactions of H_3O^+, NO^+ and O_2^+ with a series of monoterpenes, *Int. J. Mass Spectrom.*, 229, 232-240, 2003.

Schoon N., Amelynck C., Vereecken L., Coeckelberghs H., Arijs E., A selected ion flow tube study of the reactions of H_3O^+, NO^+ and O_2^+ with some monoterpene oxidation products, *Int. J. Mass Spectr.*, 239, 7-16, 2004.

Michel E., A selected ion flow tube study of the reactions of H_3O^+, NO^+ and O_2^+ with methyl vinyl ketone and some atmospherically important aldehydes, *Int. J. Mass Spectrom.*, 244/1, 50, 2005.

Amelynck C., Schoon N., Kuppens T., Arijs E., A selected ion flow tube study of the reactions of H_3O^+, NO^+ and O_2^+ with some oxygenated biogenic volatile organic compounds, submitted to *Int. J. Mass Spectrom.*, 2005.

Theoretical investigation of the OH-initiated oxidation of pinenes

Vereecken L., Peeters J., H-Atom Abstraction by OH-Radicals from (Biogenic) (Poly) Alkenes: C-H Bond Strengths and Abstraction Rates, *Chem. Phys. Lett.*, 333, 162-168, 2001.

Peeters J., Vereecken L., Fantechi G., The Detailed Mechanism of the OH-Initiated Atmospheric Oxidation of α-pinene: A Theoretical Study, *Phys. Chem. Chem. Phys.*, 3, 5489-5504, 2001.

Vereecken L., J. Peeters J., Enhanced H-atom abstraction from pinonaldehyde, pinonic acid, pinic acid and related compounds: theoretical study of the C-H bond strengths, *Phys. Chem. Chem. Phys.*, 4, 467-472, 2002.

Fantechi G., Vereecken L., Peeters J., The OH-initiated atmospheric oxidation of pinonaldehyde: detailed theoretical study and mechanism construction, *Phys. Chem. Chem. Phys.*, 4, 5795-5805, 2002.

Vereecken L., Peeters J., The 1,5-H-shift in 1-butoxy: a case study in the rigorous implementation of Transition State Theory for multi-rotamer systems, *J. Chem. Phys.*, 119, 5159-5170, 2003

Vereecken L., Peeters J., Non-traditional (per)oxy ring-closure paths in the atmospheric oxidation of isoprene and monoterpenes, *J. Phys. Chem. A.*, 108, 5197-5204, 2004.

Peeters J., Fantechi G., Vereecken L., A generalized structure-activity relationship for the decomposition of (substituted) alkoxy radicals, *J. Atmos. Chem.*, 48, 59-80, 2004.

Modeling α-pinene oxidation and the gas-particle partitioning of the products:

Capouet M., Peeters J., Nozière B., Müller J.-F., Alpha-pinene oxidation by OH: simulations of laboratory experiments, *Atmos. Chem. Phys.*, 4, 2285-2311, 2004.

Capouet M., Müller J.-F., A group contribution method for estimating the vapor pressures of α-pinene oxidation products, submitted to *Environ. Sci. Technol.*, 2005.

Reactions of oxygenated organics with OH and HO$_2$ radicals in the Upper Troposphere / Lower Stratosphere:

Vandenberk S., Vereecken L., Peeters J., The Acetic-Acid forming Channel in the Acetone + OH Reaction: a Combined Experimental and Theoretical Investigation, *Phys. Chem. Chem. Phys.*, 4, 461-466, 2002.

Vandenberk S., Peeters J., The reaction of acetaldehyde and propionaldehyde with hydroxyl radicals: experimental determination of the primary H$_2$O yield at room temperature, *J. Photochem. and Photobiol.*, 157, 269-274, 2003.

Vereecken L., Nguyen T.L., Hermans I., Peeters J., Computational study of the stability of α-hydroperoxyl- or α-alkylperoxyl substituted alkyl radicals, *Chem. Phys. Lett.*, 393, 432-436, 2004.

Hermans I., Nguyen T.L., Jacobs P.J., Peeters J., Tropopause chemistry revisited: HO$_2$-initiated oxidation as an efficient acetone sink, *J. Am. Chem. Soc.*, 126, 9908-9909, 2004.

De Smedt F., Bui X. V., Nguyen T. L., Peeters J., Vereecken L., Theoretical and experimental study of the product branching in the reaction of acetic acid with OH radicals, *J. Phys. Chem. A*, 109, 2401-2409, 2005.

Hermans I., Müller J.-F., Nguyen T.L., Jacobs P.A., Peeters J., Kinetics of alpha-hydroxy-alkylperoxyradicals in oxidation processes. HO$_2$*-initiated oxidation of ketones/aldehydes near the tropopause, *J. Phys. Chem. A*, 109, 4303-4311, 2005.

Modelling the future composition of the troposphere:

Prather M., Gauss M., Berntsen T., Isaksen I., Sundet J., Bey I., Brasseur G., Dentener F., Derwent R., Stevenson D., Lee Grenfell J., Hauglustaine D., Horowitz L., Jacob D., Mickley L., Lawrence M., von Kuhlmann M., Muller J.-F., Pitari G., Rogers H., van Weele M., Wild O., Fresh air in the 21st century? Geophys. Res. Lett., 1100, doi:10:1029/2002GL016285, 2003.

Gauss M., Myhre G., Pitari G., Prather M., Isaksen I., Berntsen T., Brasseur G., Dentener F., Derwent R., Hauglustaine D., Horowitz L., Jacob D., Johnson M., Law K., Mickley L., Muller J.-F., Plantevin P.-H., Pyle J., Rogers H., Stevenson D., Sundet J., van Weele M., Radiative forcing in the 21st century due to ozone changes in the troposphere and the lower stratosphere, J. Geophys. Res., 108, 4292, doi: 10.1029/2002JD002426, 2003.

Dentener F., and the IPCC-ACCENT modeling partners, Global air quality for the next generation, submitted to *Geophys. Res. Lett.*, 2005.

Stevenson D., and the IPCC-ACCENT modeling partners, Multi-model ensemble simulations of present-day and near-future tropospheric ozone, submitted to *J. Geophys. Res.*, 2005.

6. BIBLIOGRAPHY

Adams N.G., Smith D., Int. J. Mass Spectrom. Ion Phys., 21, 349, 1976.

Amelynck C., Schoon N., Arijs E., Int. J. Mass Spectrom., 203, 165, 2000.

Arey J., Atkinson R., Aschmann S., J. Geophys. Res., 95, 18539, 1990.

Arey J., Aschmann S., Kwok E., Atkinson R., J. Phys. Chem. A, 105, 1020, 2001.

Atkinson R., Aschmann S.M., Pitts Jr. J.N., Int. J. Chem. Kin., 18, 287, 1986.

Behforouz M., Bolan J. L. and Flyn M. S., J. Org. Chem., 50, 1180, 1985.

Calogirou A., Larsen B.R., Kotzias D., Atmos. Environ., 33, 1423, 1999.

Damian-Iordache V., Sandu A., Potra F.A., Carmichael G.R., Damian-Iordache M., The University of Iowa, Internal report, 1995.

De Hoffman E. and Stroobant V., Mass Spectrometry, Principles and Applications, Wiley, NY, p 45, 2003.

German Institute of Standardization, DIN 32645 Beuth, Berlin, 1994.

Gierczak T., Ravishankara R., Int. J. Chem. Kinet., 32, 5737, 2000.

Goudriaan J., van Laar H., Textbook with exercises (pp. 239), Kluwer Academic Publishers, Dordrecht-Boston-London, 1994.

Grosjean D., Williams E.L., Atmos. Environ., 26, 1395, 1992.

Grosjean D., Williams E.L., Seinfeld J.H., Environ. Sci. Technol., 26, 1526, 1992.

Grosjean E., Green P.G., Grosjean D., Anal. Chem., 71, 1851, 1999.

Guenther, A., Hewitt C.N., Erickson D., Fall R., Geron C., Graedel T., Harley P., Klinger L., Lerdau M., McKay W.A., Pierce T., Scholes B., Steinbrecher R., Tallamraju R., Taylor J., Zimmerman P., J. Geophys. Res., 100, 8873, 1995.

Guenther A., Karl T., Palmer P., Wiedinmyer C., Geron C., submitted to J. Geophys. Res., 2005.

Hakola H., Arey J., Aschmann S.M., Atkinson R., J. Atmos. Chem., 18, 75, 1994.

Hallquist, Wängberg I., Ljungström E., Environ. Sci. Technol., 31, 3166, 1997.

Hatakeyama S., Izumi K., Fukuyama T., Akimoto H., J. Geophys. Res., 96, 947, 1991.

Hoffmann T., Bandur R., Marggraf U., Linscheid M., J. Geophys. Res., 103, 25569, 1998.

Hoffmann T., Odum J.R., Bowman F., Collins D., Klockow D., Flagan R.C., Seinfeld J.H., J. Atmos. Chem., 26, 189, 1997.

Horowitz A., Meller R., Moortgat G., J. Photochem. Photobiol., 146, 19, 2001.

Kukui A., Borissenko D., Laverdet G., Le Bras G., J. Phys. Chem., 107(30), doi:10.1021/jp0276911, 2003.

Larsen B.R., Di Bella D., Glasius M., Winterhalter R., Jensen N.R., Hjorth J., J. Atmos. Chem., 38, 231, 2001.

Levart A., Veber M., Chemosphere, 44, 701, 2001.

Müller, J.-F., Brasseur G., J. Geophys. Res., 100, 16445, 1995.

Nozière B., Barnes I., Becker K.H., J. Geophys. Res, 104, 23645, 1999.

Orlando J., Nozière B., Tyndall G.S., Orzechowska G.E., Paulson S.E. and Rudich Y., J. Geophys. Res., 105, 11561, 2000.

Pankow, J.F., Atmos. Environ., 28, 185, 1994.

Peeters J., Boullart W., Van Hoeymissen J., Proceedings of EUROTRAC Symposium '94; P. Borrell ed., p. 110., Academic Publishing, 1994.

Peeters, J., Vereecken L., Fantechi G., Phys. Chem. Chem. Phys., 3, 5489, 2001.

Purdue L.H., Dayton D.P., Rice J., Busey J. Technical Assistance Document for Sampling and Analysis of Ozone Precursors, EPA-600/8-91-215, Research Triangle Park, NC, USA, 1991.

Rautenstrauch V., Willhalm B., Tommen W., Ohloff G., Helv. Chim. Acta, 67, 325, 1984.

Reissel A., Harry S., Aschmann S.M. Atkinson R., Arey J., J. Geophys. Res., 104, 13869, 1999.

Sellers P., Mintz Y., Sud Y., Dalcher A., J. Atmos. Sci., 43, 505, 1986.

Španěl P., Yufeng Ji, Smith D., Int. J. Mass Spectrom. Ion Processes, 165/166, 25, 1997.

Španěl P., Smith D., J. Am. Soc. Mass Spectrom., 12, 863, 2001.

Spittler M., Doctoral thesis, Bergische Universität Gesamthochschule Wuppertal, 1997.

Su T., Chesnavich W.J., J. Chem. Phys., 76, 5183, 1982.

Su T., J. Chem. Phys., 89, 5355, 1988.

Taylor P.H., *et al.*, Int. Symp. Combust. Proc., 26, 497, 1996.

Tomas A., Villenave E., Lesclaux R., J. Phys. Chem. A, 105, 3505, 2001.

Van den Bergh V., Vanhees I., De Boer R., Compernolle F. and Vinckier C., J. Chromat. A, 896, 135, 2000.

Vanhees I., Van den Bergh V., Schildermans R., De Boer R., Compernolle F., Vinckier C., J. Chromatogr. A, 915, 75, 2001.

Vasvari, G. *et al.*, Phys. Chem. Chem. Phys. 3, 551, 2001.

Vereecken L. Huyberechts G., Peeters J, J. Chem. Phys., 106, 6564, 1997.

Vereecken L., Peeters J., J. Phys. Chem. A, 103, 1768, 1999.

Vereecken L, Peeters J., Orlando J., Tyndall G., Ferronato C., J. Phys. Chem. A, 103, 4693, 1999.

Vereecken L., Peeters J., J. Phys. Chem. A, 47, 11140-11146, 2000.

Vereecken L., Peeters J., J. Chem. Phys., 119, 5159-5170, 2003.

Veyret B., Lesclaux R., Rayez M.T., Rayez J.C., Cox R.A., Moortgat G., J. Phys. Chem., 93, 2368, 1989.

Vinckier C., Compernolle F., Saleh A.M., Bull. Soc. Chim. Belg., 106, 501, 1997. .

Vinckier C., Compernolle F., Saleh A.M., Van Hoof N., Van Hees I., Fresenius Envir. Bull., 7, 361, 1998.

Wisthaler A., Jensen N.R., Winterhalter R., Lindinger W., Hjorth J., Atmos. Environ., 35, 6181, 2001.

Wollenhaupt M., Carl S.A., Horowitz A., Crowley J.N., J. Phys. Chem. A, 104, 2695, 2000.

Wollenhaupt M., Crowley J.N., J. Phys. Chem., 104, 6429, 2000.

Yu J., Cocker III D.R., Griffin R.J., Flagan R.C., Seinfeld J.H., J. Atmos. Chem., 34, 207, 1999.

Annex 1 - Acronyms and Abbreviations

Web address

4DVar	4-dimensional variational assimilation	
ACCENT	Atmospheric Composition Change:The European Network of Excellence	http://www.accent-network.org
APCI	Atmospheric Pressure Chemical Ionization	
BVOC	Biogenic Volatile Organic Compound	
CIMS	Chemical Ionisation Mass Spectrometry	
CMDL	Climate Monitoring and Diagnostics Laboratory	www.cmdl.noaa.gov
CTM	Chemistry/Transport Model	
DF – MBMS	Discharge-Flow Technique coupled to Molecular Beam Sampling Mass Spectrometry	
DFT	Density Functional Theory	
EI-MS	Electron Impact-Mass Spectrometry	
ESI	Electro-Spray Ionization	
FFR	Fast-Flow Reactor	
FFR/CIMS	Fast-Flow Reactor coupled to a Chemical Ionisation Mass Spectrometer	
FTIR	Fourier Transform Infrared	
G2M	Gaussian-2 Method	
GC-MS	Gas Chromatography-Mass Spectrometry	
HPLC	High-Performance Liquid Chromatography	
HPLC-DAD	High-Performance Liquid Chromatography- Diode Array Detection	
HPLC-MS	High-Performance Liquid Chromatography - Mass Spectrometry	
HPTFR	High-Pressure Turbulent Flow Reactor	
IMAGES	Intermediate Model for the Annual and Global Evolution of Species	
IPCC	Intergovernmental Panel on Climate Change	http://www.ipcc.ch
IPCC TAR	IPCC Third Assessment Report - Climate Change 2001	http://www.ipcc.ch
MDF	Mass Discrimination Factor	
MEGAN	Model for the Emissions of Gases and Aerosols from Nature	
MOHYCAN	Model for Hydrocarbons in the CANopy	
MOPITT	Monitoring of Pollution In The Troposphere	http://www.eos.ucar.edu/mopitt/
MS-MS	Tandem Mass Spectrometry	
PES	Potential Energy Surface	
PTR-MS	Proton-Transfer Reaction Mass Spectrometry	
RRKM	Rice Ramsperger Kassel and Marcus theory	
SARs	Structure-Activity Relationships	
SIFT	Selected Ion Flow Tube	
SLIMCAT	3-D chemical transport model	
SOA	Secondary Organic Aerosols	
TST	Transition State Theory	
UNIFAC	Universal Functional Acivity Coefficients	
URESAM	name of a computer program for unimolecular reactions	
UT/LS	Upper Troposphere/Lower Stratosphere	
UV	Ultraviolet	
UV-Visible	Ultraviolet-Visible range	
VOC	Volatile Organic Compound	

Annex 2 - Abbreviations for chemical compounds and chemical formulae

Abbreviations

Name	Description
SOA	Secondary Organic Aerosols
VOC	Volatile Organic Compound
BVOC	Biogenic Volatile Organic Compound
NMVOC	Non Methane Volatile Organic Compound
PAN	Peroxyacylnitrates
DNPH	Dinitrophenylhydrazon
PIN	Pinonaldehyde
CAR	Caronaldehyde
oxVOCs	oxygenated Volatile Organic Compounds
MVK	Methyl Vinyl Ketone
MaCR	Methacrolein

Formulae

Symbol	Name
Ar	Argon
$C_{10}H_{16}$	monoterpenes (like α- and β-pinene, Δ^3-carene and limonene)
C_5H_8	isoprene
CH_2O	formaldehyde
CH_3	methyl
$CH_3C(O)CH_3$	acetone
$CH_3C(O)OH$	acetic acid
CO	carbon monoxide
CO_2	carbon dioxide
H_2	molecular hydrogen
H_3O^+	hydronium ion
HC(O)OH	formic acid
HO_2	hydroperoxyl radical
N	nitrogen
N_2	molecular nitrogen
NO	nitric oxide
NO_2	nitrogen dioxide
NO_3^-	nitrate ion
NOx	nitrogen oxides ($NO+NO_2$)
O_2	molecular oxygen
O_2^+	dioxygen positive ion
O_3	ozone
OH^-	hydroxyl radical
ROOH	organic hydroperoxide
SF_6	sulphur hexafluoride

Annex 3 - Units

Units of the international system (SI, Système International)

Physical quantity	Name of Unit	Symbol
molar amount	mole	mol
distance	meter	m
mass	kilogram	kg
pressure	Pascal	Pa
time	second	s
energy	Joule	J
temperature	Kelvin	K
number density	molecule/m^3	molec./m^3

Prefixes, fractions and multiplication factors

Fraction	Prefix	Symbol	Multiple	Prefix	Symbol
10^{-1}	deci	d	10	deca	da
10^{-2}	centi	c	10^2	hecto	h
10^{-3}	milli	m	10^3	kilo	k
10^{-6}	micro	μ	10^6	mega	M
10^{-9}	nano	n	10^9	giga	G
10^{-12}	pico	p	10^{12}	tera	T
10^{-15}	femto	t	10^{15}	peta	P

Decimal fractions and non-SI units

Physical quantity	Name of Unit	Symbol	Definition
mixing ratio by volume	parts per million (10^6)	ppm or ppmv	
mixing ratio by volume	parts per billion (10^9)	ppb or ppbv	
mixing ratio by volume	parts per trillion (10^{12})	ppt or pptv	
pressure	atmosphere	atm	1 atm = 101300 Pa
pressure	Torr	Torr	1 atm = 760 Torr
pressure	millibar	mb	1 mb = 100 Pa
temperature	degree Celsius	°C	1 °C = 1 K, T(K)=T(°C)+273.15
latitude, longitude	degree	°	360° = 2 π radians
energy	calorie	cal	1 cal = 4.18 J
energy	kilocalorie	kcal	1 kcal = 1000 cal
number density	molecule/cm^3	molec/cm^3	
molar mass	gram per mole	g/mol	